



Available online at www.sciencedirect.com

ScienceDirect

Geochimica et Cosmochimica Acta 154 (2015) 28–48

**Geochimica et
Cosmochimica
Acta**

www.elsevier.com/locate/gca

Long-term alteration of basaltic glass: Mechanisms and rates

Benjamin Parruzot ^{a,*}, Patrick Jollivet ^a, Diane Rébiscoul ^b, Stéphane Gin ^a

^a CEA, DEN, DTCD/SECM, Marcoule, F-30207 Bagnols sur Cèze, France

^b CEA, DEN, ICSM, Marcoule, F-30207 Bagnols sur Cèze, France

Received 8 September 2014; accepted in revised form 11 December 2014; available online 22 January 2015

Abstract

The long-term behavior study of archaeological artifacts and natural minerals and glasses revealed discrepancies between laboratory and field data. For a better understanding of the cause of these discrepancies and to reinforce the use of basaltic glass as an analog for nuclear waste glasses, this study focuses on the determination of alteration rates and processes of synthetic basaltic glass in residual rate regime. Laboratory batch experiments were performed at high surface-to-volume ratios at 90 and 30 °C for more than 1000 days. In all the experiments, the residual rate regime was reached after about 6 months. The residual alteration rates at 30 and 90 °C were $4.0 \pm 1.0 \times 10^{-6}$ and $9.5 \pm 3.2 \times 10^{-6} \text{ g}\cdot\text{m}^{-2}\cdot\text{d}^{-1}$, respectively. At 90 °C, this residual alteration rate is five orders of magnitude lower than the forward alteration rate ($0.8 \text{ g}\cdot\text{m}^{-2}\cdot\text{d}^{-1}$). Altered powders and monoliths were characterized by Transmission Electron Microscopy and Time-of-Flight Secondary Ion Mass Spectrometry. From glass core to solution, the altered materials are structured as follows: pristine glass, gel (corresponding to the palagonitic layer of natural glasses) and intergranular clays. To assess the passivating properties of this alteration film, we used solid characterization, an isotopically-tagged post-leaching experiment and the measurement of mobile species diffusion coefficients through the alteration film at different stages of reaction using various techniques (solution analysis and X-ray Reflectometry). These characterizations showed that the alteration film formed during residual rate alteration is passivating even without clogged porosity within the gel. Diffusion coefficients of water and alkali metals – respectively diffusing to and from the pristine glass – through the alteration film dropped from 10^{-20} to $10^{-19} \text{ m}^2\cdot\text{s}^{-1}$ during the first alteration stages to $10^{-25} \text{ m}^2\cdot\text{s}^{-1}$ in residual rate regime.

© 2014 Elsevier Ltd. All rights reserved.

1. INTRODUCTION

Basaltic glasses are volcanic glasses found in different settings such as hyaloclastites and pillow-lavas, and in various contexts such as submarine, subglacial or lacustrine environments. Understanding their alteration mechanisms and rates is a preliminary step toward the comprehension of different natural phenomena such as volcano slope stability (Schiffman et al., 2006), the chemical mass balance of the oceans (Walton et al., 2005), and the geological history of the planet Mars (Minitti et al., 2007). This knowl-

edge may also lead to industrial applications such as geological storage of CO₂ (Stockmann et al., 2011; Gysi and Stefansson, 2012) and their use as a natural analog of nuclear glasses (Ewing, 1979; Crovisier et al., 2003; Libourel et al., 2011). In this last case, the long-term behavior of nuclear waste glasses will be predicted by building mechanistic models of their alteration (Grambow and Muller, 2001; Frugier et al., 2008) which cannot be directly validated over the long term. In order to ensure the reliability of these models, basaltic glass may be used as a natural analog whose long-term alteration mechanisms, rates and alteration conditions must be deeply investigated (Poinssot and Gin, 2012).

For nuclear glasses as well as for basaltic glasses, the first alteration step when pristine glass is immersed in

* Corresponding author. Tel.: +1 509 330 6704.
E-mail address: benjamin.parruzot@tecsomane.net (B. Parruzot).

deionized water is interdiffusion where glass modifiers cation (alkalis and, to a lesser extent, alkaline earths) diffuse outside the glass as positively charged water species diffuse inward (Boksay et al., 1967; Petit et al., 1990a; Verney-Carron et al., 2011). When dominating, this process leads to the formation of a microporous and hydrated layer called hydrated glass. In parallel to interdiffusion, hydrolysis reactions of the covalent bonds Si–O–M ($M = Si, Al, Fe, Zr, etc.$) takes place, eventually leading to the congruent release of all the elements from the glass at a maximum rate (forward alteration rate) (Techer et al., 2001; Frugier et al., 2008). As the reaction progresses, an alteration layer then forms by precipitation or condensation on the surface of the glass of elements accumulated in solution, while the alteration rate diminishes due to the decreasing affinity of the glass network hydrolysis reaction (Lasaga, 1981; Grambow, 1984; Berger et al., 1994; Daux et al., 1997; Techer et al., 2001; Oelkers and Gislason, 2001; Frugier et al., 2008) and limitation of the transport of elements through the alteration layer (Techer et al., 2001).

For nuclear glasses, the alteration rate does not drop to zero: a slowly-decreasing or constant residual alteration rate remains over time (Petit et al., 1990b; Frugier et al., 2008). This characterizes the residual rate regime which is expected to be the main regime over the long-term in sufficiently confined media and in the absence of massive precipitation of secondary minerals (Gin et al., 2013b). However, this regime has never been studied for basaltic glass. For nuclear glasses, the currently identified processes responsible for the residual rate (Frugier et al., 2008; Gin et al., 2013b) include: (1) precipitation of silicate minerals, e.g. phyllosilicates, sustaining glass network hydrolysis (Abrajano et al., 1990; Curti et al., 2006; Frugier et al., 2006; Valle et al., 2010); (2) continuation of the interdiffusion process (McGrail et al., 2001; Rebiscoul et al., 2004; Chave et al., 2007; Gin et al., 2011, 2013c) potentially slowed down by a dense layer, generally called passivating layer, displaying lower apparent diffusion coefficient than at the beginning of the corrosion process (Gin et al., 2013c). In this view, the passivating layer is expected to rapidly form during the interdiffusion process, therefore the limiting process is interdiffusion. The passivating layer dissolves at a similar rate as it forms, leading to a near constant apparent rate (Frugier et al., 2008; Gin et al., 2013c). It can be claimed that the transformation of the passivating layer into more stable compounds (porous gel and crystalline phases) is driven by thermodynamics, but the dynamics of this transformation, involving transport of reactive species and chemical reaction at nanometer and micrometer scales, remains insufficiently understood (Gin et al., 2013a). The porous gel could play a major role in the glass alteration behavior. Its restructuring over time leads to a densification (Rebiscoul et al., 2004), and even to a porosity closure in particular cases (Casey and Bunker, 1990; Cailleteau et al., 2008; Jollivet et al., 2008); crystalline phases may also precipitate in its porosities (Gin et al., 2011). The evolution of the surface species and pore size can locally affect the water mobility and reactivity (Fenter and Sturchio, 2004; Wang et al., 2006; Kerisit and Liu, 2009; Briman et al., 2012, 2013). Experimentally, the slow

residual rate has been shown to result from competing mechanisms aforementioned can last up to 15 years (Gin et al., 2012). However, under specific conditions, the high precipitation rate of particular silicate minerals such as zeolites and calcium silicate hydrates may lead to a resumption of alteration: the alteration rate increases again (Van Iseghem et al., 1984; Van Iseghem and Grambow, 1987; Ebert and Bates, 1990; Gin and Mestre, 2001; Ribet and Gin, 2004; Fournier et al., 2014).

Studies of the long-term alteration of basaltic glasses are based mainly on the examination of natural samples. The occurrence of an alteration layer generally called palagonite has been attested under various alteration conditions. This layer may be more or less crystalline and is generally associated with the presence of intergranular clays (e.g. Crovisier et al., 1992; Le Gal et al., 1999; Stronck and Schmincke, 2001, 2002; Crovisier et al., 2003). Zeolites are observed only at advanced stages of alteration at low temperatures, e.g. after 10^5 years for Icelandic samples studied by Crovisier et al. (2003), or under hydrothermal conditions (Berger et al., 1988).

The presence of a passivating layer within the alteration layer of basaltic glass has never been directly evidenced, although it has been hypothesized. For Techer et al., during alteration of synthetic basaltic glasses at high reaction progress, correct modeling of the experimental results is only possible when considering that the alteration layer slows down the release of element from the glass toward the bulk solution (Techer et al., 2001). On natural glasses, Jeong et al. considered diffusive phenomena to explain the formation of specific patterns in alteration layers on Jeju Island samples (Jeong and Sohn, 2011). Crovisier et al. consider that intergranular porosity-filling zeolites may reduce element transport from and to the glass, modifying the alteration rate and mechanisms (Le Gal et al., 1999; Crovisier et al., 2003).

Both laboratory-altered synthetic basaltic glasses and naturally-altered basaltic glasses provide data concerning long-term alteration mechanisms. However, discrepancies between laboratory and field data are observed for basaltic glass as well as for other archaeological or natural materials (Techer et al., 2001). These discrepancies must be resolved in order to better understand the long-term processes (Verney-Carron et al., 2010; Hellmann et al., 2012; Yokoyama, 2013). This study aims to determine whether or not basaltic glass undergoes a residual rate beyond saturation of the solution with respect to amorphous silica (or another polymorph controlling the equilibrium between the hydrated glass surface and the bulk solution) and if any, what could be the rate limiting mechanisms? Here are reported laboratory experiments conducted using the same protocol as for nuclear glasses (Gin et al., 2013b): they consist in long duration static test with glass powder initially placed in contact with deionized water. Between six months – the time required to reach the residual regime – and four years, concentrations of mobile species are accurately monitored and solids are characterized at the end of the tests after a short contacting time with a solution doped with exogenous tracers. Part of altered glass underwent a second short duration leaching experiment in

deionized water to evaluate the role of the alteration layer on the glass dissolution rate. In parallel, parametric experiments are conducted to determine the apparent water diffusion coefficients in pristine basaltic glass as a function of temperature and pH to determine in what extent the hydrated glass is passivating. All these experiments allow a better understanding of the rate-limiting mechanisms of basaltic glass in highly confined media.

2. MATERIALS AND METHODS

2.1. Glass preparation

Two basaltic glasses (BG) were prepared. Each was doped with an alteration tracer and named after this element: BG_{Li} was doped with the equivalent of 1 wt % Li_2O , BG_B with the equivalent of 1 wt % B_2O_3 . BG_{Li} glass had been prepared by [Techer et al. \(2000\)](#). All precursors were oxide, carbonate, oxalate and nitrate powders. After weighing, the powders were poured into a Pt-Rh crucible. Glass preparation consisted in two melts at 1500 °C with 3 h of refining. Part of the glass melt was quenched; the remainder was annealed at 700 °C. Note that the addition of B and Li to basaltic glass was justified by the fact that prior to these experiments it was not known if highly soluble elements naturally present in basaltic glass, such as Na or K, could serve as tracer at long-term. We will eventually find that Na is a good tracer.

Note also that iron(III) predominated in both BG_{Li} and BG_B glasses. This is a difference towards natural basaltic glasses where iron(II) predominates. Studies aiming to assess the effect of this difference on the alteration of the synthetic and natural glasses are still ongoing. However, none effect of this difference arised up to now ([Parruzot, 2014](#)).

Quenched BG_{Li} and BG_B glass samples were ground and milled to obtain a mean particle diameter of less than 10 µm. Fine particles were removed by washing the glass powder in absolute ethanol several times and allowing the powder to settle at appropriate times calculated using the Stoke's law. The specific surface area of the powders was measured by krypton absorption using the BET (Brunauer, Emett and Teller) method. Results were $3.98 \pm 0.20 \text{ m}^2 \cdot \text{g}^{-1}$ for BG_{Li} and $2.32 \text{ m}^2 \cdot \text{g}^{-1}$ for BG_B , with a particle size centered on 2 and 5 µm, respectively. The corresponding geometric surface area considering spherical particles would be $0.54 \text{ m}^2 \cdot \text{g}^{-1}$ for BG_{Li} and $0.28 \text{ m}^2 \cdot \text{g}^{-1}$ for BG_B .

From annealed BG_{Li} glass bar, small monoliths (approximately $5 \times 5 \times 2.5 \text{ mm}^3$) were prepared. One of their large faces was polished up to grade 4000 on SiC papers. The specimen densities were measured from the glass bars on a hydrostatic balance. Results were $2.793 \pm 0.005 \text{ g} \cdot \text{cm}^{-3}$ for BG_{Li} and $2.702 \pm 0.005 \text{ g} \cdot \text{cm}^{-3}$ for BG_B . Larger monoliths ($25 \times 8 \times 2.5 \text{ mm}^3$) were prepared for water diffusion experiments from BG_B .

Element concentrations in the glass were determined by Inductively Coupled Plasma Atom Emission Spectroscopy (ICP-AES). Two samples of each glass were dissolved, one by alkaline fusion, one by Li-tetraborate fusion. Both dissolutions were followed by neutralization by HNO_3 .

Calculated and measured compositions are indicated in [Table 1](#). The relative errors on the ICP concentrations were estimated at $\pm 5\%$ for concentrations above 1 wt %, $\pm 10\%$ below.

2.2. Leaching experiments

2.2.1. Main leaching experiments

The main leaching experiments were performed at 30 and 90 °C in static mode with a high glass-surface-area-to-leaching-solution-volume ratio (S/V ratio, m^{-1}) of 10^5 m^{-1} . Static conditions have been chosen because they allow accurate measurement of long term rates and, at least for nuclear glass SON68, it has been shown that the residual rate does not depend on the geometric parameters such as size fraction of glass powder and S/V ([Gin et al., 2013b](#)). The glass powder (6.31 g BG_{Li} powder or 10.85 g BG_B powder) was introduced in a PTFE-reactor containing 250 mL of ultrapure water (Milli-Q®, 18.2 MΩ·cm). Two small monoliths were inserted within the powder bed (BG_{Li} experiments only). All reactors were packed in a container with a few milliliters of water to minimize leaching solution evaporation. The containers were then stored in ovens at the respective leaching temperature (one test at 90 °C and one at 30 °C for both BG_{Li} and BG_B glasses) throughout the duration of the experiments. At each sampling time, the pH was measured directly in the reactor at the experimental temperature with a precision of ± 0.1 pH unit. A sample of 1.5–2 mL of leaching solution was taken and filtered through 0.45 µm filters. As the solution volume was not adjusted in the reactor after sampling, the volume decrease was taken into account when calculating normalized mass loss. Possible evaporation between samplings was also taken into account by weighing the reactor at each sampling. After 900–1000 days of main leaching experiments, a small amount of glass powders and one monolith were taken off the leaching solution, rinsed with ultrapure water and dried overnight at 50 °C. Both materials were embedded in epoxy resin and mirror polished prior to TEM characterization. BG_B glass leaching tests are still running with the remaining powder, contrary to those with BG_{Li} glass.

2.2.2. Second leaching test

Tests with BG_{Li} glass were stopped after 970 days. At this time, a second leaching test was performed with the altered powder in order in order to study how pre-altered glass behave when placed in deionized water and eventually derive an apparent diffusion coefficient of Na through the alteration layer. For that, part of the altered glass powder (1.27 g powder from BG_{Li} 90 °C, 1.70 g powder from BG_{Li} 30 °C) was rinsed in ultrapure water, allowed to settle, and then placed in a PTFE reactor containing 450 mL of ultrapure water. This test was also performed in static mode at a lower S/V ratio of $1.1 \times 10^4 \text{ m}^{-1}$ at 90 °C and $1.4 \times 10^4 \text{ m}^{-1}$ at 30 °C. The leaching temperatures and sampling method were the same as for the main leaching experiment.

Similar tests were performed with powder taken out from BG_B main leaching experiments at 906 days (1.32 g

Table 1

ICP Composition (weight %) of the basaltic glasses used for leaching experiments and STEM–EDX analysis results for BG_{Li} altered glass. For the whole table, // is used when the element is absent from this glass/alteration product. For TEM–EDX analyzes, n.d. indicates that the element was not quantified, the *italics figures* depicts the variation in composition between the glass and the alteration products (– indicates a non-significant variation). In the last line, z indicated the number of analyzed zones.

Element	BG_B Glass <i>ICP</i>	BG_{Li} Glass <i>ICP</i>	BG_{Li} Glass <i>TEM-EDX</i>	BG_{Li} Clays 90 °C <i>TEM-EDX</i>	BG_{Li} Clays 30 °C <i>TEM-EDX</i>	SON68 glass (Jollivet et al., 2012)
Si	25.4	23.0	26.0	21.7	<i>-17%</i>	21.4
Al	8.4	9.1	8.9	8.3	<i>-7%</i>	2.6
Fe	6.8	7.2	6.1	6.7	<i>+10%</i>	2.1
Ca	5.8	6.9	6.1	5.2	<i>-15%</i>	2.9
Mg	3.5	5.0	3.8	1.2	<i>-68%</i>	//
Na	1.9	1.9	2.1	n.d.	7.6	<i>+54%</i>
Ti	0.9	1.1	0.9	0.7	–	//
Li	//	0.5	n.d.	n.d.	0.9	0.9
B	0.3	//	//	//	4.4	4.4
Sr	0.3	0.3	n.d.	n.d.	0.3	0.3
K	0.2	0.2	0.1	0.3	–	//
Mn	0.1	0.1	0.1	0.1	0.2	0.2
P	0.1	< 0.1	n.d.	n.d.	0.1	0.1
Zn	//	//	//	//	2.2	2.2
Zr	//	//	//	//	2.0	2.0
Mo	//	//	//	//	1.2	1.2
Cs	//	//	//	//	1.1	1.1
Nd	//	//	//	//	1.8	1.8
Other	//	//	//	//	3.7	3.7
O	46.2	44.7	46.0	55.8	<i>+21%</i>	45.5
<i>z</i> = 6 except Na: <i>z</i> = 3				<i>z</i> = 4	<i>z</i> = 1	

from BG_B 90 °C, 1.87 g from BG_B 30 °C placed in a PTFE reactor containing 200 mL of ultrapure water. S/V ratios were $1.5 \times 10^4 \text{ m}^{-1}$ at 90 °C and $2.2 \times 10^4 \text{ m}^{-1}$ at 30 °C.

2.2.3. Apparent diffusion coefficients of water in pristine basaltic glass

Apparent diffusion coefficients of water in pristine basaltic glass as a function of temperature and pH were measured during short term experiments using the same method as Rebiscoul et al. (2007, 2012). These diffusion coefficients can be compared to those obtained previously to determine if the passivation occurs in the hydrated glass or in the alteration layer. For this, BG_B glass monoliths were altered at $S/V = 100 \text{ m}^{-1}$ in static mode in PTFE reactors. Two series of experiments were performed. The first one consisted in 5 experiments at pH = 3 with temperatures equal to 4; 30; 40; 50 and 60 °C. The second one consisted in 6 experiments at 30 °C with pH equal to 0; 1; 2; 3; 4 and 5. The pH was measured at the temperature of the experiment and adjusted using HCl (Prolabo® ‘Normapur®’) with a precision of ± 0.1 pH units. Before alteration, the solution was placed in an oven at the temperature of the experiment during 24 h. Durations were comprised between a few minutes and a few hours. For such short alteration duration the concentrations in the leachate are too low to be measured by classical solution analysis method. For each alteration, the same glass monolith was taken from the reactor, rinsed with ultrapure water, dried at the laboratory atmosphere, analyzed and then reimmersed in its leachate. Two surface characterization techniques were used: X-ray Reflectometry (XRR) in order to determine the altered glass thickness and Fourier's transform infrared spectrometry in attenuated

total reflectance mode (FTIR-ATR, not reported here) to confirm that glass network hydrolysis did not predominate over glass hydration (Rebiscoul et al., 2012). Hydrolysis predominance was observed for experiments attempted at pH values higher than 5.

2.3. Solution analyses results processing

2.3.1. Alteration rate calculation

All sampled solutions were acidified to $0.1\text{--}0.5 \text{ mol}\cdot\text{L}^{-1}$ HNO_3 (Merck® Suprapur®) in preparation for ICP analyses. The analyses were performed on a Thermo® Scientific iCAP Duo ICP-AES instrument. Five elements were analyzed in all sampled solutions: Na, Mg, Si, K and Li or B (for BG_{Li} or BG_B experiments respectively). Ca, Al, P, Ti, Mn and Fe were only analyzed in a few samples. The quantification limit for all the considered elements was 10 ppb. The uncertainty on the measured value varied depending on the measured concentration: 40% up to 100 ppb; 20% from 100 to 200 ppb; 10% from 200 ppb to 2 ppm; 5% from 2 to 3 ppm; 3% above 3 ppm.

The normalized glass mass loss ($NL(i,t)$, $\text{g}\cdot\text{m}^{-2}$, Eq. (1)) was calculated with respect to each analyzed element at each sampling time:

$$NL(i,t) = \frac{m(i,t)}{\tau_i \times S} \quad (1)$$

where $m(i,t)$ (given by Eq. (2), in grams) represents the total mass of element i released in solution at time t (days), τ_i is the mass fraction of element i in the glass (Table 1), and S the leached powder surface area (m^2). $m(i,t)$ comprises two terms: the first represents the mass of element i present in

the leachate at time t , the second is the sum of the masses of element i sampled for the previous solution analyses:

$$m(i, t) = [i]_t \times V_{L,t} + \sum_{t_n=0}^{t-1} [i]_{t_n} \times V_{S,t_n} \quad (2)$$

where $[i]_t$ ($\text{g}\cdot\text{L}^{-1}$) is the concentration of element i in solution at time t , $V_{L,t}$ is the volume (L) of leachate in the PTFE reactor at time t , and V_{S,t_n} is the volume (L) sampled for solution analyses at time t_n .

From $NL(i, t)$, different parameters can be calculated such as the equivalent thickness ($ET(i, t)$, μm , Eq. (3)), the retention factor ($RF(i/Tr, t)$, unitless, Eq. (4)), and the alteration rate ($r(i)$, $\text{g}\cdot\text{m}^{-2}\cdot\text{d}^{-1}$, Eq. (5)):

$$ET(i, t) = \frac{NL(i, t)}{\rho_g} \quad (3)$$

where ρ_g is the glass density ($\text{g}\cdot\text{cm}^{-3}$).

$$RF(i/Tr, t) = \frac{1 - NL(i, t)}{NL(Tr, t)} \quad (4)$$

where $NL(Tr, t)$ is the normalized mass loss for a tracer element Tr , typically alkali metals or boron.

$$r(i) = \frac{dNL(i, t)}{dt} \quad (5)$$

When calculating a residual rate from Eq. (5), two assumptions can be made depending on the tracer's behavior during the residual rate regime. (a) a constant residual rate versus time is assumed, which would indicate that glass network hydrolysis is the predominant alteration mechanism. In this case, $NL(i, t)$ is proportional to t as shown by Eq. (6):

$$NL(i, t) = a_L \times t + b_L \quad (6)$$

where a_L is the slope and b_L is the y -intercept of the linear regression. In this case, the residual alteration rate (r_r , $\text{g}\cdot\text{m}^{-2}\cdot\text{d}^{-1}$, Eq. (7)) is the slope:

$$r_r(i) = a_L \quad (7)$$

(b) the rate decreases proportionally to the square root of time, indicating a predominance of diffusion over dissolution in the residual rate domain as depicted by Eq. (8):

$$NL(i, \sqrt{t}) = a_{sq} \times \sqrt{t} + b_{sq} \quad (8)$$

where a_{sq} is the slope and b_{sq} is the y -intercept of the linear regression. This $t^{-0.5}$ dependent residual rate may also be expressed as a diffusion coefficient (D_i , $\text{m}^2\cdot\text{s}^{-1}$, Eq. (9)) using the method presented by Chave et al. (2007):

$$D_i = \frac{a_{sq}^2 \times \pi}{4\rho_g^2} \quad (9)$$

The quality of the regressions lines is assessed using their determination coefficient, R^2 .

2.3.2. Geochemical calculations

The geochemical calculations were performed with the Chess geochemical code (van der Lee et al., 2003) using the CTDP thermodynamic database (CTDP, 2004). Silica species taken into account were mainly H_4SiO_4 , HSiO_3^- and NaHSiO_3 . $\text{H}_2\text{SiO}_4^{2-}$ can be estimated but remains very

low due to the pH. Polymers and other colloids potentially present in the leachates were not taken into account experimentally or by calculation. In particular, pH were calculated and compared to experimental pH. An uncertainty of ± 0.2 – 0.3 pH units had to be considered on the calculated pH values, arising mainly from the fact that some elements released from the glass (e.g. Ca) were not analyzed in all sampled solutions and could not be included in pH calculations.

2.4. Solid characterization

2.4.1. Residual rates experiments

After 900–1000 days of main leaching experiments, part of the powders and one monolith were separated from the leaching solution and dried overnight at 50 °C. Both materials were embedded in epoxy resin and mirror-polished.

2.4.1.1. Focused ion beam. FIB milling was performed with a FEI® 200 TEM FIB system at the University of Aix-Marseille. We used the procedure described by Benzerara et al. (2007). The FIB cross section was prepared with a 30 kV Ga^+ beam operating at ≈ 20 nA. The prepared cross section measuring approximately $12 \times 5 \times 0.15 \mu\text{m}^3$ was transferred at atmospheric pressure with a micromanipulator to the membrane of a carbon-coated 200 mesh copper grid. Five FIB cross-sections were prepared using this technique: one for each of the altered powders and one for the altered BG_{Li} 90 °C monolith.

2.4.1.2. TEM and EDX Analyses. Two Transmission Electron Microscopes (TEM) were used in the analyses. The morphological observations were made on a JEOL® JEM 2010F microscope operating at 200 kV, equipped with a field emission gun, a high-resolution UHR pole piece, and a Gatan®GIF200 energy filter. Energy-Dispersive X-ray (EDX) analyses were carried out on a Technai®G2 (FEI) equipped with a LaB_6 source operating at 200 kV. The detectors were a Gatan® CCD camera, a STEM BF-DF detector, and an EDAX® Genesis for the EDX analyses. The spatial resolution was 0.27 nm.

2.4.1.3. Time-of-Flight Secondary Ion Mass Spectrometry. ToF-SIMS was used to determine the elemental profiles within the alteration layer. Two altered monoliths from the BG_{Li} 90 °C and BG_{Li} 30 °C main leaching experiments were rinsed in ultrapure water. A tracing solution enriched in isotopes ^{29}Si , ^{18}O and ^2H was prepared and its pH, Na and Si composition were adjusted to the values obtained for the final sample of the BG_{Li} 90 °C main leaching test. Monoliths were dipped into this tracing solution for 24 h, then rinsed and dried for 24 h at 90 °C. A TOF IV ToF-SIMS apparatus from IONTOF® was then used to measure the elemental profiles in the alteration layer on the monoliths. Abrasion was carried out using a 1 keV primary O^{2+} ion beam with a current of 200 nA when analyzing cations and a 1 keV primary Cs^+ ion beam with a current of 80 nA when analyzing anions. Both abrasion areas measured $350 \times 350 \mu\text{m}^2$. Analysis was performed using a 25 keV Bi^+ ion beam at 1.3 pA on an area measuring

$80 \times 80 \mu\text{m}^2$. The surface charge was neutralized on the monoliths by a pulsed low-energy (<20 eV) electron flux. All the element intensity values I were normalized with respect to the signal for the $^{209}\text{Bi}^+$ ion to avoid possible matrix effects. To mitigate the effect of primary current variations, the intensity of each isotope was normalized with respect to the main isotope of the glass and gels, i.e. ^{28}Si . The results for each element nX at each analysis cycle i are presented normalized with respect to the pristine glass in the form of a C/C_0 ratio (Eq. (10)):

$$[C/C_0({}^nX)] = \frac{\left[\frac{I({}^nX)}{I({}^{28}\text{Si})} \right]_i}{\left[\frac{I({}^nX)}{I({}^{28}\text{Si})} \right]_{\text{pristine glass}}} \quad (10)$$

The depth calibration of the elemental profiles was determined by final profilometer measurement of the crater depth. A constant abrasion rate was assumed throughout the analyzed material.

2.4.2. Water diffusion coefficient in the glass

The glass monolith's surface was characterized by X-ray Reflectometry (XRR) to determine the density and the thickness of the altered glass zone. XRR apparatus is a Bruker® D8 diffractometer using $\text{CuK}_{\alpha 1}$ ($\lambda = 0.154056 \text{ nm}$) radiation and standard $\theta-2\theta$ scan for the data collections. This technique was used to determine the thickness and the density of the glass altered zone from the electron density profiles as a function of the depth. These were obtained from the fits of the experimental curves using the Firefx4c_6 software (Ober, raymond.ober@college-de-france.fr) based on the Parratt algorithm (Parratt, 1954) adjusting the electron densities of n layers on a substrate. For our samples, we used the model proposed by Rebiscoul et al. (2007, 2012) given uncertainties of $\pm 3 \text{ \AA}$ for the thickness. Regarding the numerous fitting results obtained in this study, we will only present the total thickness of the altered zone.

From the evolution of the glass altered zone thickness (x , m), which is proportional to $t^{0.5}$ as long as diffusive

processes predominated over hydrolysis of the glass network, apparent water diffusion coefficient (D_i , $\text{m}^2 \cdot \text{s}^{-1}$) can be calculated using Eq. (11), derived from Fick's first law, by regression of $e_i = f(t^{0.5})$:

$$D_i = \frac{\pi \times x^2}{4t} \quad (11)$$

3. RESULTS

In the following sections, two distinct terms are used to designate the alteration products. *Alteration layer* refers to the inner part of the alteration film comprising the gel and the hydrated glass. *Alteration film* refers to the alteration layer and the diffuse layer of clays (i.e. all alteration products). All these zones are schematically represented on Fig. 1.

3.1. Main leaching experiments

3.1.1. Solution analyses

Results from solution analyses from the main leaching experiments for both glasses at both temperatures of 30 and 90 °C are reported in Table 2.

The pH variation versus time is shown on Fig. 2. The observed patterns all followed two successive steps: a rapid initial increase in the pH followed by a steady-state regime differing from one experiment to another. The rapidly-increasing pH was not always clearly visible, in particular for BG_{Li} 30 °C. However, as the water was initially pure in all the experiments, the pH at t_0 was neutral to slightly acidic (this acidification eventually originates from atmospheric CO_2 solubilization in the water). All the first measured pH values were above $\text{pH} = 9$, clearly showing a rapid increase in the first hours or days of alteration. After 90–180 days, all the pH variations had stabilized. Two main trends were then observed: at 90 °C the pH was stable or slightly increasing; at 30 °C it decreased. Throughout the experiments, the pH values were 0.5–1 unit lower for BG_{B} than for BG_{Li} at 90 °C as well as at 30 °C.

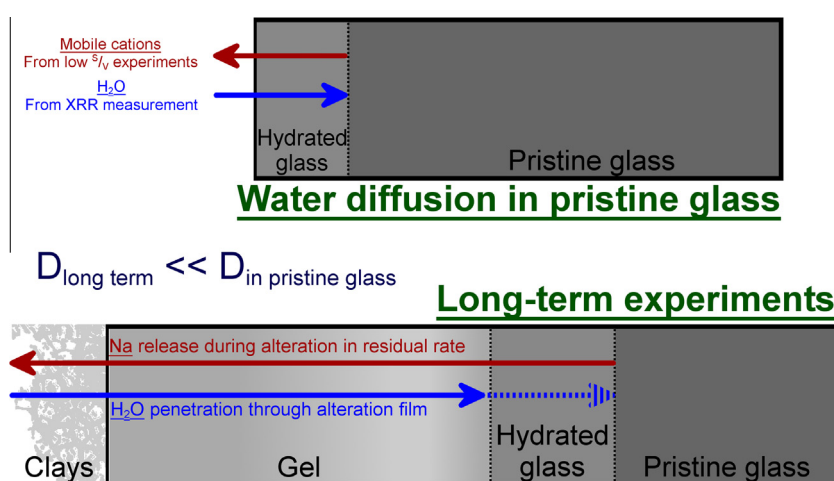


Fig. 1. Schematic representation of the basaltic glass alteration films. Up: alteration film of basaltic glass during water diffusion in the pristine glass experiments Down: alteration film of the basaltic glass during long-term experiments. Water diffusion towards the glass is depicted by blue arrows, alkali metal release from the glass is depicted by red arrows. (For interpretation of the references to colour in this figure legend, the reader is referred to the web version of this article.)

Table 2

pH, element concentrations, and calculated $\text{H}_4\text{SiO}_4^0_{(\text{aq})}$ concentrations for the main leaching experiments. Values below quantifications limits are reported in italics with QL indicated.

Time (d)	pH ^{T°C}	[Na] (ppm)	[Li] (ppm)	[Si] (ppm)	[Mg] (ppm)	Calculated pH ^{T°C} with dissolved CO ₂	Calculated [$\text{H}_4\text{SiO}_4^0_{(\text{aq})}$] (mmol·L ⁻¹)
<i>BG_{Li} 90 °C</i>							
7	9.56	61.8	13.1	35.2	0.21	9.08	0.332
14	9.63	71.2	13.8	37.6	0.24	9.11	0.313
49	9.69	87.8	14.0	40.9	0.18	9.16	0.302
94	9.69	91.8	13.4	44.9	0.20	9.16	0.330
182	9.76	84.2	11.6	45.4	<i>0.02^{QL}</i>	9.12	0.294
368	9.84	91.5	10.1	53.0	<i>0.02^{QL}</i>	9.12	0.293
552	9.70	88.6	8.4	53.6	<i>0.03^{QL}</i>	9.10	0.388
781	10.12	94.7	10.1	63.7	<i>0.03^{QL}</i>	9.12	0.197
970	9.81	114.8	9.9	69.9	<i>0.25^{QL}</i>	9.13	0.389
<i>BG_{Li} 30 °C</i>							
7	10.56	18.2	6.0	7.1	1.58	8.46	0.041
14	10.56	21.2	6.7	8.2	1.90	8.48	0.047
49	10.31	25.5	8.0	7.9	0.96	8.54	0.072
94	10.32	28.7	8.9	7.8	0.81	8.58	0.069
182	10.22	29.0	8.9	7.9	0.40	8.59	0.083
368	10.03	22.8	8.4	6.2	0.83	8.51	0.088
552	9.83	30.2	7.3	5.5	1.56	8.62	0.099
781	9.59	31.3	9.7	5.6	1.40	8.62	0.121
970	9.38	36.1	9.8	5.1	1.85	8.66	0.121
Time (d)	pH ^{T°C}	[Na] (ppm)	[B] (ppm)	[Si] (ppm)	[Mg] (ppm)	Calculated pH ^{T°C} with dissolved CO ₂	Calculated [$\text{H}_4\text{SiO}_4^0_{(\text{aq})}$] (mmol·L ⁻¹)
<i>BG_B 90 °C</i>							
1	9.04	36.3	5.8	25.5	0.12	8.67	0.514
3	9.09	46.4	7.9	31.2	0.06	8.74	0.592
7	9.23	51.7	9.2	33.5	0.07	8.77	0.536
14	9.28	57.3	10.4	34.3	<i>0.03^{QL}</i>	8.80	0.513
28	9.26	62.2	11.5	35.7	<i>0.03^{QL}</i>	8.83	0.547
53	9.24	68.3	12.7	37.0	<i>0.03^{QL}</i>	8.86	0.579
182	9.16	79.7	14.5	38.8	<i>0.34^{QL}</i>	8.91	0.669
365	9.18	85.1	15.8	50.0	<i>0.03^{QL}</i>	8.95	0.838
553	9.21	99.9	17.7	63.1	<i>0.03^{QL}</i>	8.96	1.011
780	9.22	96.6	17.5	78.0	<i>0.05^{QL}</i>	8.92	1.236
906	9.27	94.8	18.7	98.2	<i>0.03^{QL}</i>	8.85	1.418
1142	9.19	102.4	20.2	122.4	<i>0.01^{QL}</i>	8.84	1.952
<i>BG_B 30 °C</i>							
1	9.77	6.5	0.6	3.3	2.2	7.93	0.067
3	9.96	12.2	1.4	5.1	3.0	8.15	0.082
7	9.95	14.6	1.8	6.7	3.7	8.23	0.109
14	9.99	16.2	2.1	6.8	3.8	8.26	0.105
28	9.88	18.6	2.3	6.8	4.2	8.31	0.120
53	10.10	24.4	3.2	8.1	55	8.42	0.105
182	9.41	25.8	3.4	6.0	8.0	8.49	0.160
365	8.96	28.8	4.0	6.3	12.5	8.62	0.204
553	8.80	32.3	4.1	5.8	15.8	8.77	0.193
780	8.80	31.1	3.9	5.5	18.1	8.78	0.184
906	8.78	32.9	4.7	6.1	19.0	8.77	0.200
1142	8.73	36.2	4.7	7.7	20.7	8.82	0.253

The behavior of all analyzed elements was the same up to 90 days: NL for all elements increased rapidly during the first days of alteration before a release rate drop was observed. After 90–180 days of alteration, the NL variation slowed down and differed depending on the glass (Fig. 3), the temperature and the element analyzed.

3.1.1.1. Alkali metals and boron. Na, Li and B exhibited similar behavior in almost all our experiments. A notable exception was the BG_{Li} 90 °C experiment where a slightly decreasing NL(Li) was observed, indicating a probable consumption of Li from solution into alteration products. The choice of Na as a tracer for all experiments is discussed in the next section.

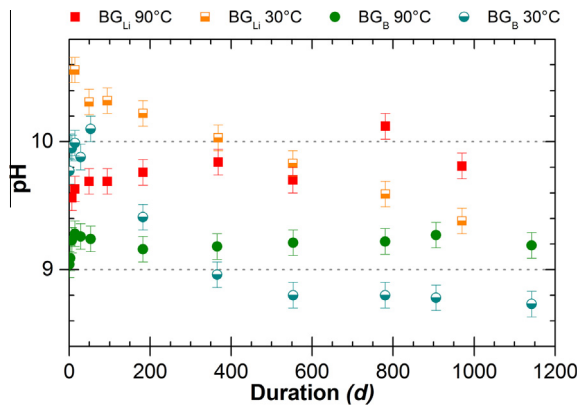


Fig. 2. pH versus time during the main leaching experiments for both glasses (BG_B , circles; and BG_{Li} , squares) at both temperatures (90 °C, filled symbols; and 30 °C, half-filled symbols).

3.1.1.2. Silicon. It is a major component of both the glass and the alteration layers of basaltic glass. $NL(Si)$ was 1–2 orders of magnitude lower than $NL(Na)$ or $NL(B)$ in all experiments, corresponding to a retention factor in the alteration products for Si exceeding 95%.

Three concomitant phenomena will be considered when analyzing the evolution of Si release in solution: $H_4SiO_4(aq)$ release through glass hydrolysis (Fig. 3 and Table 2), Si consumption through precipitation and in situ condensation reactions (formation of the gel and the secondary phases in the alteration film) and the acid-base equilibrium between $H_4SiO_4(aq)$ and $HSiO_3$. Saturation towards amorphous silica was not attained in any of the experiments at any time. At 90 °C in the residual rate domain, the pH was constant as $NL(Si,t)$ and concentration of $H_4SiO_4(aq)$ increased: hydrolysis was still ongoing. The amount of Si released through hydrolysis was greater than the amount of Si consumed through precipitation of secondary phases. At 30 °C, $NL(Si,t)$ decreased: the amount of Si released through hydrolysis was smaller than the consumption of Si through secondary phase precipitation. A shift in the acid-base equilibrium caused the concentration of $H_4SiO_4(aq)$ to increase during the pH drop even though the total Si concentration decreased. This pH drop may be explained by atmospheric CO_2 solubilization. The PTFE reactors used here were not totally hermetic to gas exchange: the leaching solution may have dissolved atmospheric CO_2 and become acidified. When considering our solutions at equilibrium with atmospheric CO_2 (considered

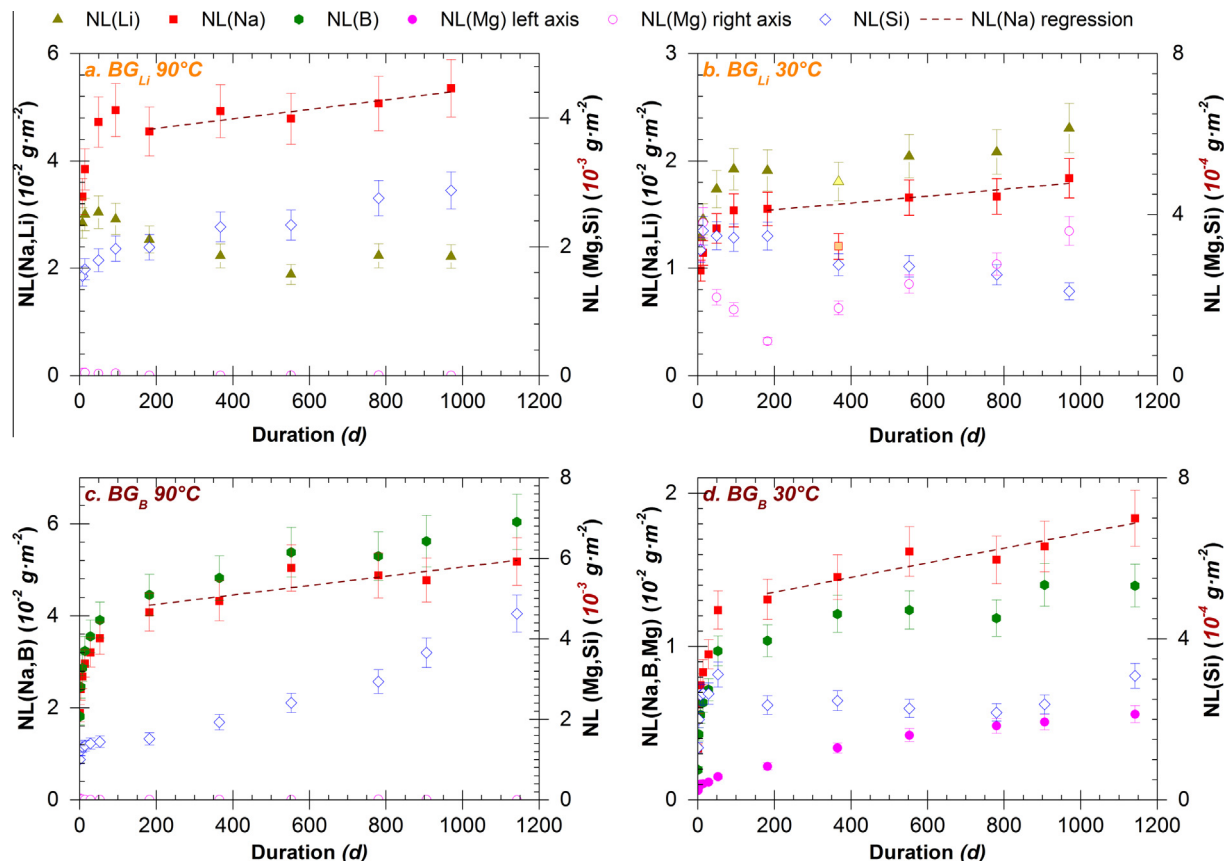


Fig. 3. Normalized mass losses versus time for BG_{Li} and BG_B main leaching experiments. Left axis, filled symbols: $NL(Na)$, red squares; $NL(Li)$, green triangles; $NL(B)$, green hexagons and $NL(Mg)$, magenta circles (BG_B 30 °C only). Right axis, empty symbols: $NL(Si)$, blue diamonds and $NL(Mg)$, magenta circles (all experiments except BG_B 30 °C only). Brown dashed line represents $NL(Na)$ regression versus time on the residual rate domain. (For interpretation of the references to colour in this figure legend, the reader is referred to the web version of this article.)

Table 3

Concentrations and retention factors for most elements present in the glass, at 1142 days for BG_B experiments. Values below quantifications limits are reported in italics with QL indicated.

Element	90 °C – 1142 days		30 °C – 1142 days	
	Concentration (ppm)	Retention factor	Concentration (ppm)	Retention factor
Si	122.4	91%	7.7	98%
Na	102.4	–	36.2	–
B	20.2	\approx 0%	4.7	23%
Mg	0.01^{QL}	\approx 100%	20.7	70%
Al	6.64	99%	0.28	\approx 100%
Ca	3.46	99%	21.8	75%
P	0.06	99%	0.28	77%
Sr	0.09	\approx 100%	0.55	88%
Ti	0.01^{QL}	\approx 100%	0.01^{QL}	\approx 100%
Mn	0.01^{QL}	\approx 100%	0.01^{QL}	\approx 100%
Fe	0.01^{QL}	\approx 100%	0.01^{QL}	\approx 100%

atmospheric value: 370 ppm CO₂ (Lide, 2005)), the pH values calculated with Chess software at each time point (Table 2) indicated that both 30 °C leachates tended toward this equilibrium with increasing time. Finally, the measured pH for the BG_B 30 °C experiment appeared to stabilize: equilibrium was reached with atmospheric CO₂. Differences from one experiment to another may be explained by the variable degree of sealing of the PTFE reactors. It is important to note that no carbonated secondary phases were observed during solid characterizations (e.g. calcite, magnesite, siderite (Stockmann et al., 2011)).

3.1.1.3. Other elements. Mg was retained in the alteration film. At 90 °C, Mg retention was almost total as $NL(Mg)$ was 2–3 orders of magnitude lower than $NL(Na)$. At 30 °C, $NL(Mg)$ was 5–50 times lower than $NL(Na)$. As for Si, the Mg retention factors generally exceeded 95%. One notable exception was for BG_B at 30 °C where the retention factors ranged from approximately 70% to 90%. Ca, like Mg, exhibited higher retention during BG_B 90 °C experiment than during BG_B 30 °C after 553 days of alteration with retention factors of respectively 98% and 67%. Most other major elements (Al, Fe, Ti) were almost fully retained in the alteration layer after 1142 days of alteration (Table 3).

3.1.2. Features of the alteration film

Alteration films were observed with TEM–EDX (Fig. 4). Observations of the powders were similar for BG_{Li} and BG_B experiments. An alteration film was observed for both ultrathin sections prepared from resin-coated altered powder samples (Fig. 4c and d) in the form of secondary phases precipitated on the glass surface. These low-density phases were probably poorly crystallized clays. Clays are commonly observed as basaltic glass alteration products (Crovisier et al., 2003). The secondary phases were dispersed in form of aggregates but no uniform alteration layer was observed on ultrathin sections prepared from resin-coated powder samples. The alteration film of the BG_{Li} 90 °C altered monolith was also characterized

(Fig. 4a and b). A 40–80 nm thick continuous amorphous layer covered the monolith (Fig. 4b). However, its density appears to be close to that of the glass and the interface between the two materials was difficult to identify. This layer is porous and poorly crystalline clays are observed in the voids (Fig. 4b, internal part of alteration layer). It was possible to measure the interplanar spacing on some of these clayey filaments: the mean interplanar spacing for 9 measurement zones was 13.2 Å, which corresponds to the spacing measured in natural palagonites, thus indicating that these clays could be di- or trioctahedral smectites such as nontronites or saponites (Stroncik and Schmincke, 2002; Crovisier et al., 2003). A 10–15 nm layer split apart during the resin coating (Fig. 4b, precipitate layer) and may correspond to precipitates formed during the drying step prior to resin coating.

The chemical composition of the glass and of the clays was measured (Table 1) by Energy Dispersive X-ray (EDX) spectrometry. Within uncertainties, the glass composition obtained by EDX is similar to the glass composition obtained by ICP analyses. The clays were enriched in oxygen, which could be explained by the greater hydration of this layer compared to the pristine glass.

3.1.3. Distribution of elements through the alteration film

The distribution of the elements through the alteration layer was evaluated through the ToF-SIMS characterization of altered BG_{Li} monoliths by focusing on the profile of (a) mobile elements released from the glass and (b) specific elements penetrating from the solution into the alteration film during a tracing experiment. These profiles are shown in Fig. 5.

It is important to note that the x-axis scale is only indicative, as we assumed a constant abrasion rate of the materials during the ToF-SIMS analysis. However, the abrasion rate is expected to vary with the different densities of the materials forming the alteration layer. As shown by the TEM analyses (Fig. 4), clays encountered at the alteration layer surface had a low density which makes them easily abraded. We could consider that the thick layer of clays would appear as the first 10–20 analyzed nanometers at 90 °C, the first 5 analyzed nanometers at 30 °C but due to the much lower density of the clays, this value is an underestimate of their real thicknesses.

Li and Na were released from the glass but both were partly retained in the alteration layer as shown by previous analyses (solution, TEM). In both cases, a certain degree of retention was also observed by ToF-SIMS analysis (Fig. 5). In the inner part of the alteration layer, neither Na nor Li profiles were sharp at both leaching temperatures: the C/C_0 ratio for both alkali metals slowly decreases. This could be attributable either to a slow transport by diffusion of those elements through the alteration layer or to an artifact due to the mixing between pristine glass and alteration layer signals. This artifact is quite common: it comes from the interfacial roughness and the tilt angle between the sputtering beam and the surface of the sample. Li retention increased again when moving toward the surface: the C/C_0 ratio reached a max-

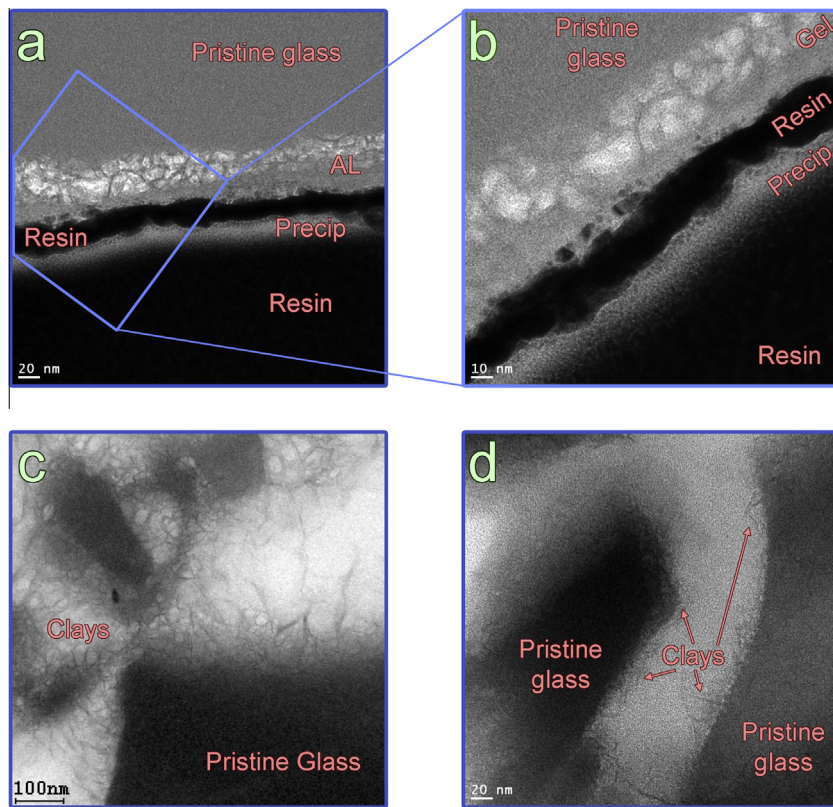


Fig. 4. TEM Observations: (a) and (b) HR-TEM on BG_{Li} 90 °C-altered monolith; (c) HR-TEM on BG_B 90 °C-altered powder; (d) HR-TEM on BG_{Li} 30 °C-altered powder. Abbreviations: AL = Alteration Layer, Precip. = Precipitate.

imum of 0.5 at 90 °C and 0.2 at 30 °C near the surface. This confirmed the higher retention of this element at 90 °C compared with 30 °C. Na showed a similar – but less pronounced behavior – at 90 °C where a plateau is observed at $C/C_0 \approx 0.1$.

From the profiles of elements released by the glass, the interfaces were represented by dashed lines on Fig. 5 and were situated at a mid- C/C_0 height between the plateaus. The alteration film thickness could be estimated as 50–66 nm at 90 °C and 13–18 nm at 30 °C depending on the chosen element, Na or Li.

Fig. 5 also shows how fast tagged water $\text{H}_2^{[18]\text{O}}$ and tagged silica $\text{H}_4^{[29]\text{Si}}\text{O}_{4(\text{aq})}$ diffuse through the previously formed alteration film. The penetration of these two molecules was measured by comparison with isotopes already present in the alteration film and originating from the glass (^{28}Si and ^{16}O) and the main leaching solution (^{16}O). Both signals showed a positive C/C_0 ratio and their profiles converge to $C/C_0 = 1$ at the same depth than the mobile species released by the glass. According to the ToF-SIMS profiles it can be concluded that, after 970 days of alteration, the porosity of the alteration film was open and sufficient for $\text{H}_4^{[29]\text{Si}}\text{O}_{4(\text{aq})}$ and $\text{H}_2^{[18]\text{O}}$ to penetrate through most of the alteration layer. The experimental uncertainty hinders from determining precisely to which interface this convergence point corresponds (glass/hydrated glass, hydrated glass/alteration layer, or both together).

3.2. Second leaching experiments with altered glass samples

This section presents the results of the diffusion leaching experiment in which powder samples altered for 900–1000 days were leached again in pure water. It was thus possible to estimate the apparent diffusion coefficient through the alteration film of the sodium, mobile element released from the glass. The concentrations and pH values measured at each sampling interval are indicated in Table 4. The evolution of $NL(\text{Na}) - NL(\text{Si})$ was plotted versus the square-root of time in Fig. 6. By subtracting $NL(\text{Si})$ from the normalized mass loss of glass alteration tracer, the contribution of hydrolysis to alteration of the glass and alteration products is disregarded. The remaining difference $NL(\text{Na}) - NL(\text{Si})$ represents the diffusion contribution to alteration.

For BG_{Li} , values before $40 \text{ s}^{0.5}$ at 90 °C and before $80 \text{ s}^{0.5}$ at 30 °C (Fig. 6, domain A) were constant: at this stage, diffusion is not measurable. However, another fast phenomenon seemed to occur during the first minute of alteration, during which all elements were released at a high rate: this could be due to release of the remaining dissolved species within the porosity of the alteration layer. Domain A was not observed for BG_B secondary leaching experiments. At both temperatures, $NL(\text{Na}) - NL(\text{Si})$ then increased proportionally with $t^{0.5}$ (Fig. 6, domain B). In this domain, alteration predominantly occurred by diffusion of the considered elements. The release of the considered

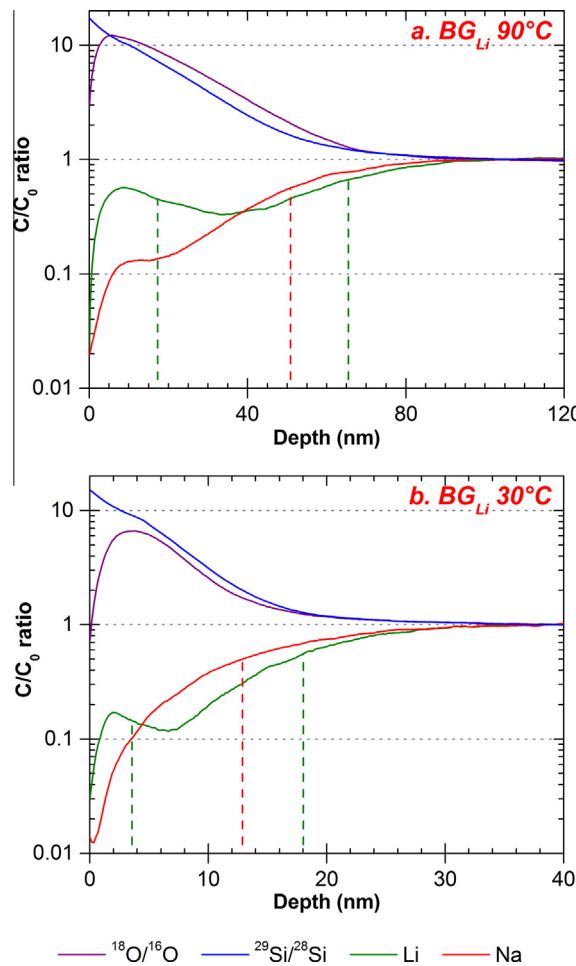


Fig. 5. Time-of-Flight Secondary Ion Mass Spectroscopy (ToFSIMS) profiles for some isotopes diffused from solution (^{18}O and ^{29}Si) as well as alkali metals released during alteration (Li, Na). Profiles are normalized with respect to the main isotope of the glass and gels, i.e. ^{28}Si , and with respect to the pristine glass in the form of a C/C_0 ratio (Eq. (10)).

elements appeared to slow down after a few days (Fig. 6, domain C).

Using the method of Chave et al. (2007), the sodium diffusion coefficients D_{Na} through the alteration film were calculated using Eq. (9) and the slope from the linear regression of $[\text{NL}(\text{Na}) - \text{NL}(\text{Si})] = f(t^{0.5})$ on domain B. For BG_{Li} , D_{Na} is $7.7 \times 10^{-22} \text{ m}^2 \cdot \text{s}^{-1}$ at 90°C and $4.9 \times 10^{-25} \text{ m}^2 \cdot \text{s}^{-1}$ at 30°C . For BG_{B} , D_{Na} is $4.3 \times 10^{-21} \text{ m}^2 \cdot \text{s}^{-1}$ at 90°C and $2.5 \times 10^{-24} \text{ m}^2 \cdot \text{s}^{-1}$ at 30°C .

3.3. Apparent water diffusion coefficients in pristine glass

The goal of these measurements was to determine the apparent water diffusion coefficients in the pristine glass and their variation with the temperature and pH of the solution. Water transport rates in the glass and mobile cations release rates through the resulting alteration layer were determined and compared to literature data and to the residual alteration rates.

Hydrated glass thicknesses were obtained from the fit of the X-ray Reflectivity data provided as Appendix A to this article. The evolutions of hydrated glass thicknesses followed a linear behavior as a function of the square root of time for the two series of experiments (variable temperature: pH = 3 at $4\text{--}60^\circ\text{C}$; variable pH: 30°C at pH = 0 to pH = 5) as presented on Fig. 7a and b. These evolutions are characteristic of a diffusive process. Thus, the apparent water diffusion coefficients ($D_{\text{H}_2\text{O}}$, $\text{m}^2 \cdot \text{s}^{-1}$) were calculated using Eq. (11), and reported in Table 5a. These diffusion coefficients are of the same order of magnitude than those obtained for SON68 glass or simple borosilicate which are comprised between 10^{-24} and $10^{-20} \text{ m}^2 \cdot \text{s}^{-1}$ (Rebiscoul et al., 2007, 2012), and 4–5 orders of magnitude inferior to helium – an atom similar in size as water but not reactive regarding the silicate network – diffusion coefficient in the SON68 glass at the same temperature (Chamssidine et al., 2010; Fares et al., 2011). This difference suggests that the low apparent water diffusion coefficients are probably due to the glass structure and chemical interactions with glass components. For example, the higher Ca amount in basaltic glass than in SON68 glass can lead to the strengthening of the glass structure and to the formation of strong complexes between Ca and water slowing down the water diffusion through the glass network (Indris et al., 2005).

$D_{\text{H}_2\text{O}}$ at pH = 3 evolves with temperature according to an Arrhenius law as shown on Fig. 7c. The activation energy is equal to $43.2 \pm 3.6 \text{ kJ} \cdot \text{mol}^{-1}$, that is approximately two times less than for simple borosilicate glasses ($76.9 \text{ kJ} \cdot \text{mol}^{-1}$ (Rebiscoul et al., 2007)) or three times less than for SON68 glass ($133 \pm 27 \text{ kJ} \cdot \text{mol}^{-1}$ (Rebiscoul, 2014)). This difference may also arise from composition and structure of the basaltic glass. Indeed, basaltic glass contains less mobile elements such as alkali metals or boron than the SON68 glass (Table 1).

The effect of pH on $D_{\text{H}_2\text{O}}$ of basaltic glass is characterized by a drop of one order of magnitude of $D_{\text{H}_2\text{O}}$ between pH = 1 and pH = 4 as shown on Fig. 7d which corresponds to the point of zero charge of amorphous silica around pH = 2–3. However, the point of zero charge for a basaltic glass is much higher, comprised between pH = 6.8 at 25°C and pH = 6.1 at 50°C (Guy and Schott, 1989). The best mathematical fit to represent $D_{\text{H}_2\text{O}}$ (30°C) evolution between pH = 0 and pH = 5 is given by Eq. (12)

$$D_{\text{H}_2\text{O}}(30^\circ\text{C}) = 1.29 \cdot 10^{-21} + \frac{3.28 \cdot 10^{-20}}{1 + e^{\frac{\text{pH}-1.77}{0.41}}} \quad (12)$$

In order to be compared to previously published data acquired in similar experimental conditions (low S/V, short durations), our dataset is recalculated at neutral pH over a wider range of temperatures. Using the water diffusion coefficient at pH = 5 and 30°C calculated from Eq. (12) and making the assumption that this value does not evolve at higher pH, the water diffusion coefficient at neutral pH and at 30°C is estimated at $1.3 \times 10^{-21} \text{ m}^2 \cdot \text{s}^{-1}$. Assuming that the activation energy determined on Fig. 7c does not vary with pH, the corresponding water diffusion coefficient at 90°C would be $2.2 \times 10^{-20} \text{ m}^2 \cdot \text{s}^{-1}$.

These values can be compared to alkali metals diffusion coefficients measured by Verney-Carron et al. (2011) or

Table 4

Solution analysis results for the second leaching experiments (altered glasses in pure water). Values below quantifications limits are reported in italics with Q_L indicated.

BG _{Li} 90 °C					BG _{Li} 30 °C				
Time (mn)	pH	[Na] (ppm)	[Li] (ppm)	[Si] (ppm)	Time (mn)	pH	[Na] (ppm)	[Li] (ppm)	[Si] (ppm)
1	8.17	0.68	0.06	0.42	1	8.05	0.33	0.06	0.22
5	8.19	0.67	0.07	0.52	5	7.95	0.22	0.05	0.12
10	8.10	0.66	0.06	0.51	10	7.94	0.25	0.06	0.08
15	8.11	0.76	0.07	0.50	15	7.28	0.39	0.06	0.07
30	8.26	1.43	0.12	1.51	30	7.58	0.27	0.06	0.12
60	8.31	1.88	0.14	1.93	60	7.61	0.28	0.06	0.09
180	8.41	2.89	0.21	4.14	180	7.80	0.26	0.06	0.14
420	8.49	4.23	0.33	7.58	420	7.57	0.37	0.07	0.23
1440	8.66	5.55	0.52	14.01	1440	7.79	0.53	0.09	0.87
4320	8.75	6.34	0.67	17.54	4320	7.76	0.64	0.10	1.49
10,000	8.79	6.73	0.76	18.43	10,000	7.82	1.03	0.14	2.42
BG _B 90 °C					BG _B 30 °C				
Time (mn)	pH	[Na] (ppm)	[B] (ppm)	[Si] (ppm)	Time (mn)	pH	[Na] (ppm)	[B] (ppm)	[Si] (ppm)
7	8.11	0.35	0.01	0.21	6	8.11	0.04	<i>0.01Q_L</i>	0.01
15	8.30	1.43	0.03	0.96	14	8.23	0.04	<i>0.01Q_L</i>	0.03
33	8.50	2.33	0.03	1.59	30	7.90	0.09	<i>0.01Q_L</i>	0.05
60	8.53	3.08	0.03	2.06	60	8.28	0.09	<i>0.01Q_L</i>	0.07
180	8.41	3.92	0.04	3.89	191	8.18	0.24	<i>0.01Q_L</i>	0.13
420	8.51	4.46	0.08	7.18	426	8.62	0.42	0.02	0.58
1440	8.53	5.86	0.32	15.5	1440	8.33	0.51	0.02	1.00
4328	8.56	6.69	0.45	17.8	4303	8.36	0.63	0.03	1.59
9977	8.70	6.57	0.48	11.5	9950	8.02	0.80	0.05	2.24

data published by Petit et al. (1990a) from which diffusion coefficients may also be calculated based from alkali metal depletion depths using Eq. (11). These diffusion coefficients are reported in Table 5b and are of the same order of magnitude than the extrapolated water diffusion coefficients in the pristine glass. However, an activation energy of 65.8 kJ·mol⁻¹ was determined for alkali-metal diffusing from pristine glass, different from the 42.8 kJ·mol⁻¹ for water diffusion into the glass. This is surprising because water penetration is normally anticorrelated to alkali metals release (Doremus, 1975; Petit et al., 1990b; Frugier et al., 2008). However, pH were different for both datasets (acidic pH for ours, slightly basic for Verney-Carron et al. and Petit et al.) and some hydrolysis occurrence was acknowledged by Verney-Carron et al. Both of these changing parameters may cause a difference in alteration mechanisms and thus different activation energies (unlike the assumption made previously).

In consequence, and in order to compare the apparent water penetration coefficients to the other diffusion coefficients presented in this study, we considered the following approximation: data at a pH as close as possible from neutrality (pH = 5) was used and the same activation energy was used at pH = 5 than at pH = 3.

4. DISCUSSION

According to the most documented theory on glass corrosion, two coupled mechanisms control the residual alteration rate of nuclear glass: (1) interdiffusion, involving water transport from solution to the pristine glass and

diffusion through the alteration film of species arising from glass dissolution; (2) precipitation of silicate phases, generally crystalline (Abrajano et al., 1990; Gin and Mestre, 2001; Gin et al., 2004, 2011, 2012; Curti et al., 2006; Frugier et al., 2006, 2008; Valle et al., 2010). Recent studies have shown that the transport of aqueous species within the alteration film can be affected by pore closure in the gel (Jollivet et al., 2008; Cailleteau et al., 2008), and/or by silica saturation of the pore solution in the interdiffusion zone (Maeda et al., 2012; Gin et al., 2013b,c). The precipitation of secondary phases consumes network-forming elements (Si, Al, Fe, etc.) from the layers considered to be protective, and becomes a driving force that sustains glass dissolution. Another approach has been proposed these last years to revisit glass dissolution mechanisms (Geisler et al., 2010; Hellmann et al., 2012; Dohmen et al., 2013): the key processes are the congruent dissolution of the glass whatever the reaction progress and the leaching conditions and the in situ precipitation of the less soluble elements at the reaction front to form alteration products (gel, crystalline phases).

In the following sections we determine the residual rate of basaltic glass and discuss how the processes mentioned above could be applicable to basaltic glasses.

4.1. Residual rate determination

4.1.1. Choice of a tracer

The alteration rate is calculated from the element concentrations in solution. It is therefore necessary to designate an element released from the glass that will be considered as

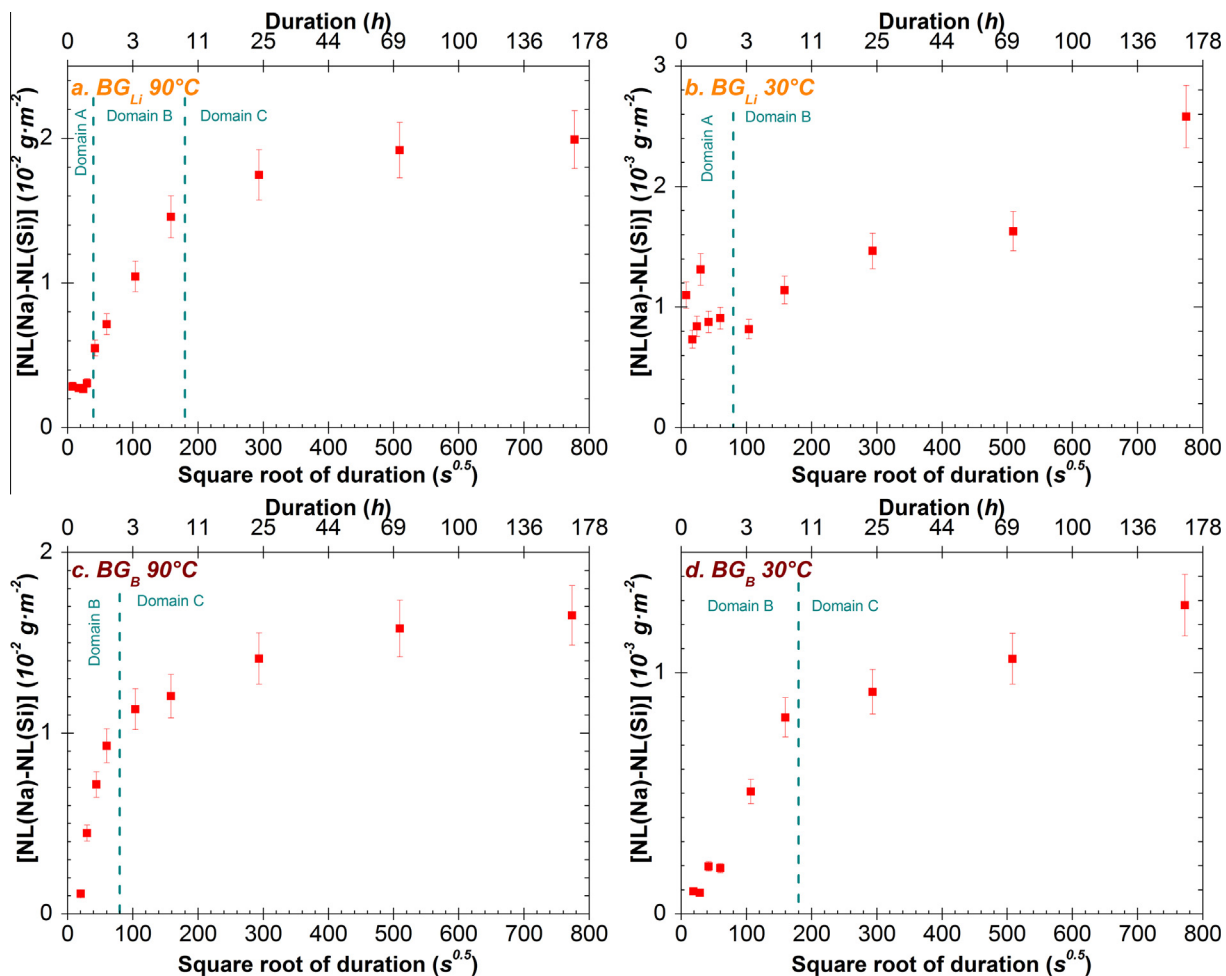


Fig. 6. $NL(i)-NL(Si)$ versus the square-root of time for the second leaching experiment with altered glass samples. $NL(Na)-NL(Si)$: red squares, $NL(Li)-NL(Si)$: green triangles; $NL(B)-NL(Si)$: green hexagons. (For interpretation of the references to colour in this figure legend, the reader is referred to the web version of this article.)

an alteration tracer during the experiments. A suitable tracer element must be sufficiently soluble to avoid retention in the alteration film or reprecipitation in solution. The alkali metals (Na, Li, K) and boron are generally considered to be good glass alteration tracers (Techer et al., 2001; Frugier et al., 2008; Jeong and Sohn, 2011).

In this study, the low potassium content of the glass and the contamination of the solution by the KCl electrode used to measure the pH in the reactor at each sampling interval prevented us from using the K concentrations in solution.

Lithium has previously been used as a dopant in synthetic basaltic glasses and was considered to be a satisfactory tracer (Daux et al., 1997; Techer et al., 2001). However, during experiment BG_{Li} 90 °C, the $RF(Li/Na)$ value after 182 days and the low drop of the C/C_0 ratio of the ToF-SIMS profile in the alteration film (Fig. 5) indicate approximately 50% Li retention in the alteration products. Li had the highest normalized mass loss at 30 °C, and could be considered the best tracer at this temperature. However, this affirmation is tempered by the ToF-SIMS profile of this element (Fig. 5), which is similar to the shape of the profile at 90 °C, although C/C_0 values for Li retention at 30 °C were much lower than at 90 °C.

Boron is frequently used as an alteration tracer in borosilicate glasses (e.g. nuclear glasses (Frugier et al., 2008)). It is not incorporated in the alteration products except under hydrothermal conditions (Scheetz et al., 1985) or at $pH \geq 12$ (Mercado-Depierre et al., 2013). Boron was used as a dopant for the BG_B experiments, and constitutes a satisfactory tracer at both temperatures. Its retention compared with sodium was equivalent to the experimental error. Although it is a good alteration tracer, boron was not present in all the experiments reported here. Therefore, to ensure consistency, it was not selected for this purpose.

Sodium is found naturally in basaltic glass. During weathering in the natural environment, it is only slightly retained in the alteration layer and in clays (Jeong and Sohn, 2011), regardless of whether the mass balance is calculated at constant volume or in comparison to an element considered as immobile – commonly Fe – (Crovisier et al., 1992; Stroncik and Schmincke, 2002). However, zeolite precipitation – naturally observed in specimens unexposed to hydrothermal conditions older than 10^5 years except under hydrothermal conditions (Le Gal et al., 1999) – or alteration in seawater (Stroncik and Schmincke, 2002; Walton et al., 2005) – may result in the incorporation of Na from

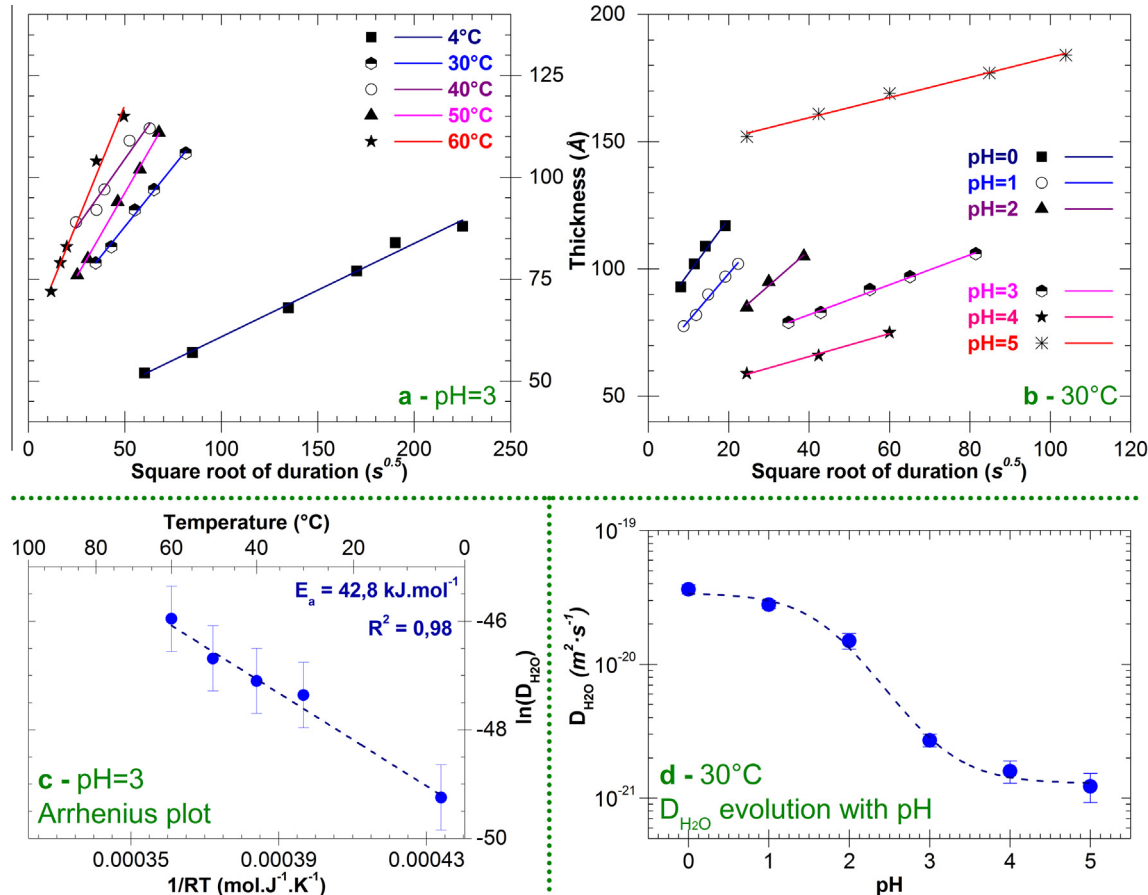


Fig. 7. Water diffusion in pristine glass. Up: evolution of the altered thicknesses as a function of the square root of time for (a) experiments at $pH^T°C = 3$ with variable temperatures and (b) experiments at 30 °C with variable pH. Down: (c) Arrhenius plot of the evolution of water diffusion coefficient in the pristine glass at $pH^T°C = 3$ and (d) Evolution of the water diffusion coefficient in the pristine glass as a function of the pH at 30 °C.

Table 5

Apparent diffusion coefficients (a) of water in the pristine glass and (b) of alkali metals from the pristine glass.

(a) Apparent water diffusion coefficients into pristine basaltic glass (this study)

Series of experiments	Temp (°C)	Initial $pH^T°C$	S/V (m ⁻¹)	Duration (h)	D_{H_2O} (m ² ·s ⁻¹)
Variable temperature $pH = 3$	4	3	0.01	14.1	$(4.1 \pm 0.5) \times 10^{-22}$
	30	3	0.01	1.85	$(2.7 \pm 0.3) \times 10^{-21}$
	40	3	0.01	1.10	$(3.5 \pm 0.5) \times 10^{-21}$
	50	3	0.01	1.25	$(5.3 \pm 1.0) \times 10^{-21}$
	60	3	0.01	0.68	$(1.1 \pm 1.0) \times 10^{-20}$
Variable pH 30 °C	30	0	0.01	0.10	$(3.6 \pm 0.3) \times 10^{-20}$
	30	1	0.01	0.14	$(2.8 \pm 0.2) \times 10^{-20}$
	30	2	0.01	0.42	$(1.5 \pm 0.2) \times 10^{-20}$
	30	4	0.01	1.00	$(1.6 \pm 0.3) \times 10^{-21}$
	30	5	0.01	3.00	$(1.2 \pm 0.3) \times 10^{-21}$

(b) Alkali metal diffusion coefficients from pristine glass towards solution

Experiment	Temp (°C)	Initial $pH^T°C$	S/V (m ⁻¹)	Duration (d)	D_{Li} (m ² ·s ⁻¹)	D_{Na} (m ² ·s ⁻¹)
PW-90*	90	Neutral	70	3.8	5.3×10^{-20}	7.7×10^{-20}
PW-50*	50	Neutral	78	2	2.4×10^{-21}	—
Basaltic Glass†	120	Neutral	2	0.56	$D_{H_2O} = 1.6 \times 10^{-19} \text{ m}^2 \cdot \text{s}^{-1}$	

* With data from Verney-Carron et al. (2011).

† With data from Petit et al. (1990a).

solution into the alteration products, but here sodium may be considered as a good tracer for all the leach tests performed in this study. It is found at higher concentrations in the glass than the other elements considered above. $RF(Na/Li)$ beyond 182 days for experiment BG_{Li} 30 °C was of the order of the experimental error. However, TEM–EDX analysis indicated a doubling of the Na concentration in clay compared with the pristine glass. The quantity of Na retained in the clays is nevertheless negligible compared with the amount dissolved, given the low density of the clays observed both in the alteration layer (Fig. 4a and b) and on its surface (Fig. 4c and d).

Since it is present in all the experiments and only slightly retained in the glass alteration products, sodium is selected as the alteration tracer for all the experiments.

4.1.2. Residual rate domain delimitation

In static tests at high S/V ratios, such as the experiments discussed here, glass alteration at the forward rate is estimated to last a few seconds to hours depending on temperature before the rate diminishes (Gin et al., 2013b). The rate drop is attributed to saturation of the solution with respect to a silicate phase limiting the transport of aqueous species (Techer et al., 2001), and can be approximated by a first-order law expressing the decreasing affinity toward $H_4SiO_4^{(aq)}$ activity in solution (Grambow, 1984) as described by Gin et al. (2012). The experimental data were fitted with

a first-order law, as defined by Eq. (13) where r_0 is the forward dissolution rate ($\text{g} \cdot \text{m}^{-2} \cdot \text{d}^{-1}$) and $a_{H_4SiO_4}^*$ the activity of silica at equilibrium with respect to hydrated glass (Galeczka et al., 2014).

$$r = r_0 \left(1 - \frac{a_{H_4SiO_4}}{a_{H_4SiO_4}^*} \right) \quad (13)$$

Up to about 180 days the experimental data points follow a first-order law (Fig. 8) before they begin to deviate. The difference from saturation of silicic acid at the glass surface is then no longer sufficient to quantify glass alteration.

It is noteworthy that the shape of the curve is the same for different borosilicate glasses compositions from simple to complex, such as SON68 nuclear glass (Gin et al., 2012), differing only by the time t_r at which the inflection is observed. Irrespective of the differences among the glass compositions investigated here, t_r was generally shorter than observed by Gin et al. (2012). This can be attributed to the higher S/V ratio used in our experiments: the higher the S/V , the sooner the rate drops. The inflection point corresponds to the beginning of the residual rate regime after 180 days. Even if the instantaneous rate may fluctuate slightly, the residual rate regime is then assumed to persist as long as no change occurs in the limiting mechanism (e.g. precipitation of specific minerals that may lead to a sudden

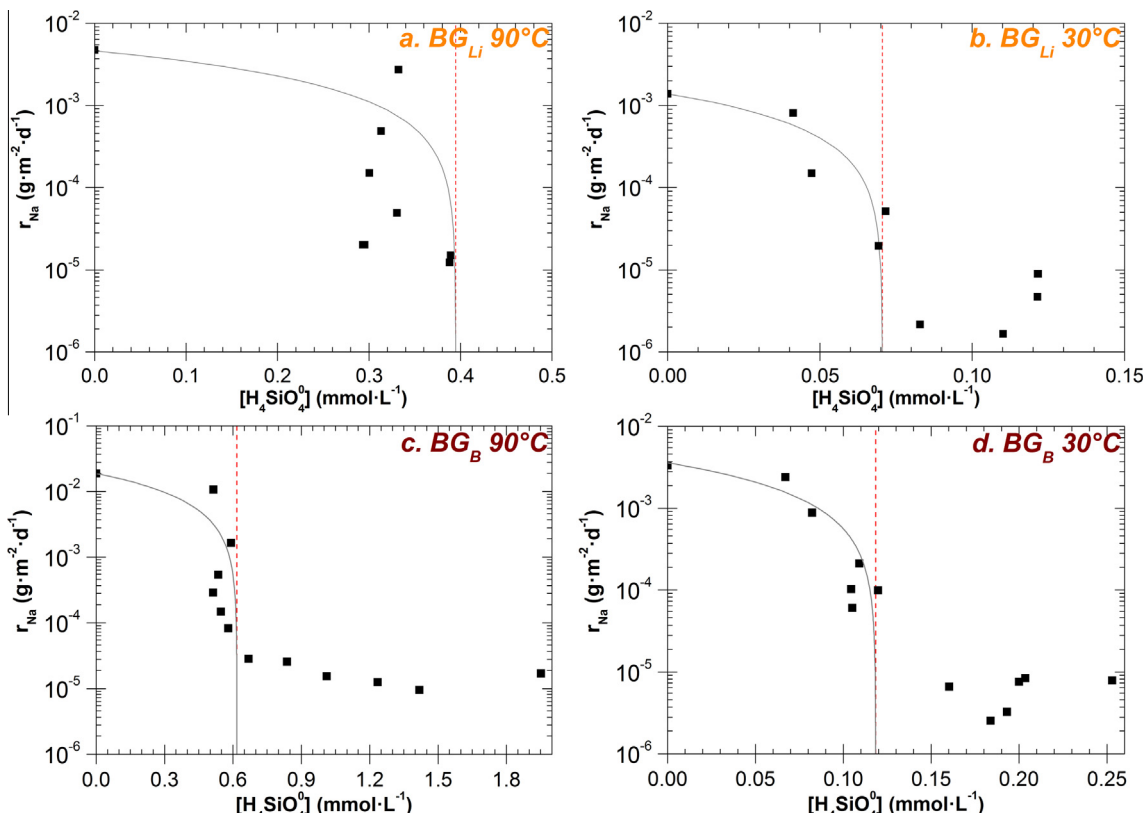


Fig. 8. Alteration rate versus orthosilicic acid concentration for all four main leaching experiments (BG_B and BG_{Li} at 90 and 30 °C). Black squares: experimental data. Continuous line: first-order rate law computer according to Eq. (13) whose corresponding saturation concentration is represented as a red dashed line. (For interpretation of the references to colour in this figure legend, the reader is referred to the web version of this article.)

resumption of alteration). All the saturation concentrations obtained from the first-order law (red dashed lines on Fig. 8) are inferior to the solubility limit of silica in similar conditions.

The inflection point cannot be determined for experiment BG_{Li} 90 °C. This could be due to the pH fluctuations measured during this experiment (Fig. 2). Near the pK_a value of the $H_4SiO_4(aq)/HSiO_3^-$ couple ($pK_a \approx 9.2$ at 90 °C), a slight pH variation results in a significant variation in the $H_4SiO_4(aq)$ concentration. The data point at 780 days indicating a relatively large variation in the pH, and thus in the $H_4SiO_4(aq)$ content, was ignored since no sudden changes were observed for the element concentrations in solution (in particular for the alkali metals). As the temperature and the nature of the dopant did not appear to affect t_r for the other three experiments, we also considered that the residual rate conditions began after 180 days for experiment BG_{Li} 90 °C and then persisted until the end of the experiment.

4.1.3. Computation of residual rates

The starting point of the residual rate regime is considered to be defined by the turning point of the experimental curve from the first-order rate law. For our experiments, this occurred after approximately 180 days. In consequence, all experimental points before 180 days were ignored to compute residual rates.

Because of the experimental uncertainties, two residual alteration rates were computed for all experiments by regression of the experimental data for $NL(Na) = f(t)$. These two rates correspond to the two possible assumptions presented previously: a constant residual rate (shown as a dashed line on Fig. 3) with Eqs. (6) and (7), or a $t^{-0.5}$ -decreasing residual rate with Eqs. (8) and (9). Respective residual rate (r_r , g·m⁻²·d⁻¹) and diffusion coefficient values (D_{Na} , m²·s⁻¹) are given in Table 6. At 90 °C, the residual rate of the synthetic basaltic is approximately five orders of magnitudes lower than the forward alteration rate of BG_{Li} glass equal to 0.8 g·m⁻²·d⁻¹ published by Techer et al. (2000).

Considering the equal regression quality (quantified by the R^2 factor, in Table 6), it is not possible to conclude solely from solution analysis about which of the hydrolysis or interdiffusion processes predominates during basaltic glass alteration in residual rate regime.

4.2. Processes occurring during alteration in residual rate

The Transmission Electron Microscopy observations and ToF-SIMS characterization showed that the alteration films on samples BG_{Li} 30 °C and BG_{Li} 90 °C were qualitatively similar: from the pristine glass outward to solution, they comprised an amorphous alteration layer (Fig. 4a and b) and secondary minerals (Fig. 4c and d). The issue here is to determine the role of the alteration film in the onset and persistence of a residual alteration rate. For borosilicate complex and simple glasses, it has been shown that the alteration film can inhibit the release of elements (Gin et al., 2011) or even form a barrier preventing access to water (Cailleteau et al., 2008; Jollivet et al., 2008). For this last consideration, ToF-SIMS experiments (Fig. 5) were performed and revealed that the porosity of the alteration film is open and allows penetration of water (blue arrow, Fig. 1b). However, imprecisions arising from ToF-SIMS analysis hinder from precisely determining the diffusion coefficients of mobile species (e.g. water and alkali elements) in the passivating zone, near the pristine glass/alteration film interface (dashed part of blue arrow on Fig. 1b).

The protective effect of the alteration layer on glass dissolution rate can also be evaluated thanks the measurement of the apparent diffusion coefficient of mobile species through this layer. If the diffusion coefficient is lower than the apparent water diffusion coefficient in the pristine glass, then reactive transport of aqueous species through the alteration layer is rate limiting.

All diffusion coefficients presented in this study are compared on Fig. 9. Values were extrapolated as close as possible to temperature and pH conditions encountered in our long-term experiments as explained previously.

Because water species (H_2O , H_3O^+ ...) ingress into the pristine glass is followed by the release of alkali metals to insure electrical balance – this process is called interdiffusion – both species generally display anti-correlated profiles corresponding to similar diffusion coefficients (Boksay et al., 1967; Doremus, 1975). This is confirmed in our case when comparing both apparent diffusion coefficients of water into the pristine glass (Fig. 9, * bar and blue arrow on Fig. 1a) and alkali metal release from the basaltic glass (Fig. 9, ° bar and red arrow on Fig. 1a) which are of the same order of magnitude (differences may arise from the difference between the glasses and the experimental methods).

Table 6

Residual rate values when considering a t -dependent law (left) and Na diffusion coefficients when considering a $t^{0.5}$ -dependant law, for all main experiments. For each mean, the largest uncertainty of the two values is used.

Experiment	$NL(i, t) = a_L \times t + b_L$		$NL(i, \sqrt{t}) = a_{sq} \times \sqrt{t} + b_{sq}$	
	r_r (g·m ⁻² ·d ⁻¹)	R^2	D_{Na} (m ² ·s ⁻¹)	R^2
BG_{Li} 90 °C	$8.9 \pm 2.2 \times 10^{-6}$	0.847	$1.8 \pm 0.1 \times 10^{-25}$	0.830
BG_{Li} 30 °C	$3.1 \pm 1.0 \times 10^{-6}$	0.840	$3.3 \pm 0.3 \times 10^{-26}$	0.785
BG_B 90 °C	$1.0 \pm 0.3 \times 10^{-5}$	0.647	$3.1 \pm 0.2 \times 10^{-25}$	0.713
BG_B 30 °C	$4.8 \pm 0.9 \times 10^{-6}$	0.860	$6.5 \pm 0.2 \times 10^{-26}$	0.867
Mean 90 °C	$9.6 \pm 3.2 \times 10^{-6}$	–	$2.5 \pm 0.2 \times 10^{-25}$	–
Mean 30 °C	$4.0 \pm 1.0 \times 10^{-6}$	–	$4.7 \pm 0.3 \times 10^{-26}$	–

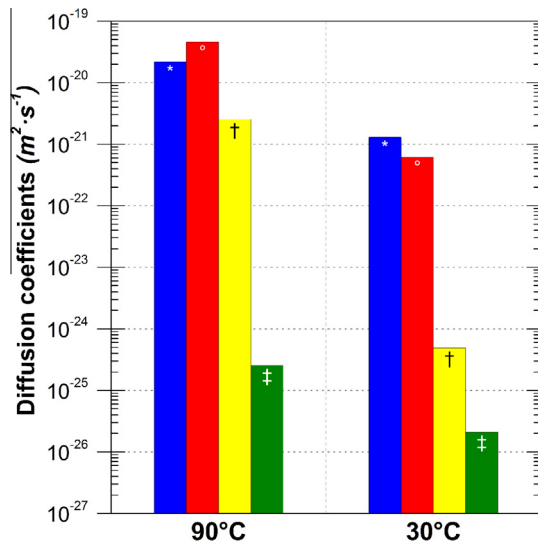


Fig. 9. Comparison of all the diffusion coefficients presented in this article. Blue bars with * symbol: water diffusion coefficients into the BG_B glass. Red bars with ° symbol: alkali metals diffusion coefficients from the glass, extrapolated from literature data. Yellow bars with † symbol: Na diffusion coefficients from the second leaching experiments on altered glass, mean for BG_Li and BG_B at each temperature. Green bars with ‡ symbol: Na diffusion coefficients in residual rate regime, mean for BG_Li and BG_B at each temperature. (For interpretation of the references to colour in this figure legend, the reader is referred to the web version of this article.)

The water penetration rate in the glass can be calculated by mean of Eq. (11) at 900 days and compared to the residual rate. Values at 90 °C are 300 and $1.3 \text{ nm} \cdot \text{y}^{-1}$, respectively (72 and $0.5 \text{ nm} \cdot \text{y}^{-1}$ at 30 °C). This difference of two orders of magnitude indicates that the water penetration rate is not the single residual rate limiting process and that another phenomenon limits the interaction between the solution and the glass.

The diffusion coefficients of alkali metals released by the glass through the alteration layer obtained from the secondary leaching experiments (Fig. 9, † bar) show contrasted results: they are 3–4 orders of magnitude superior to residual-rate diffusion coefficients at 90 °C, 1–2 orders of magnitude superior to residual-rate diffusion coefficients at 30 °C. Ultrapure water was used for these experiments and may have caused a dissolution of the alteration layer (in particular when considering the higher difference between the diffusion coefficients at 90 °C than at 30 °C, the predominance of hydrolysis being more important at 90 °C) or a modification of the concentration gradient between the bulk solution and the interface with the glass. Thus, diffusion coefficients from secondary leaching experiments may not be used for further comparison.

The short term diffusion coefficients ($D_{\text{H}_2\text{O}}$) determined in the absence of an alteration layer are 4–5 orders of magnitudes larger than alkali metal diffusion coefficients through the alteration film in residual rate regime (Fig. 9, ‡ bar and red arrow on Fig. 1b). Considering that no dense layer (porosity clogging) was observed in the alteration layer and that most of the porosity is open even after 900 days of

alteration, if a transport limiting zone is present then it is very thin (a few nanometers?) and could not be observed. Considering also that at low reaction progress, a hydrated glass layer (Fig. 1a) was characterized by XRR and leads to diffusive release of alkali metals from the glass, the following hypotheses can be assumed concerning the constitution of the passivating layer:

- Either, the passivating layer is constituted of a thin hydrated glass layer at the pristine glass/alteration film interface and of a dense zone at the innermost part of the gel as for the SON68 glass (Yanagisawa et al., 1997; Rebiscoul et al., 2005). Both play a barrier role, limiting water transport and chemical species transport between the glass and the solutions.
- Or, the passivating layer is constituted of the sole hydrated glass (or a part of it), as for SON68 nuclear glass or ISG simple glass. However, this hypothesis does not explain the rate variation between short and long term. Local pH variations inducing a chemistry different in the bulk than in the solution confined into the porosity of the alteration film may provide an explanation (Briman et al., 2013).

5. CONCLUSION

Synthetic basaltic glass was altered in the laboratory for more than 1000 days. At high reaction progress and under saturation towards hydrated glass conditions, synthetic basaltic glasses undergo alteration in residual rate regime. This residual alteration rate was quantified for the first time and the processes involved during this residual alteration rate regime were partly clarified. Rates were determined to be $9.6 \times 10^{-6} \text{ g} \cdot \text{m}^{-2} \cdot \text{d}^{-1}$ at 90 °C and $4.0 \times 10^{-6} \text{ g} \cdot \text{m}^{-2} \cdot \text{d}^{-1}$ at 30 °C. From pristine glass to solution, the alteration film is made of a passivating layer, a gel layer and clayey secondary phases. Processes involved during alteration at residual rate comprise of a continued hydrolysis of the glass due to secondary phase precipitation and a limitation towards element transport through the alteration layer. This limitation is likely imposed by a very thin passivating layer which has not yet been characterized but is probably composed of hydrated glass and/or a dense gel layer.

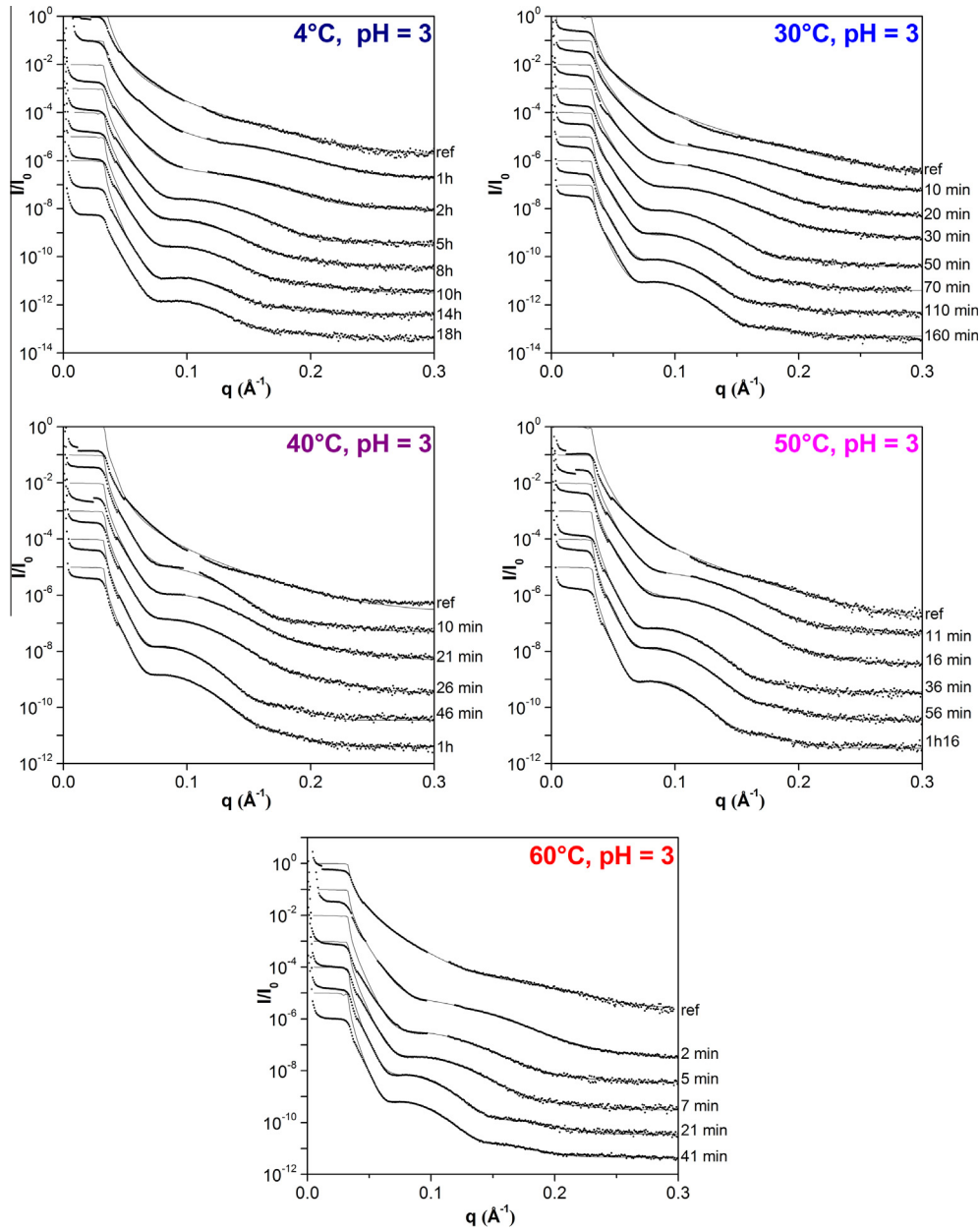
These results provide a deeper understanding of basaltic glasses long term alteration rates and mechanisms, and may be compared to samples formed and altered naturally. The results of this study are also valuable when considering basaltic glass as a natural analog of nuclear glasses: the similarities of mechanisms and rates in residual rate regime may permit the extension of the analogy to even longer time periods.

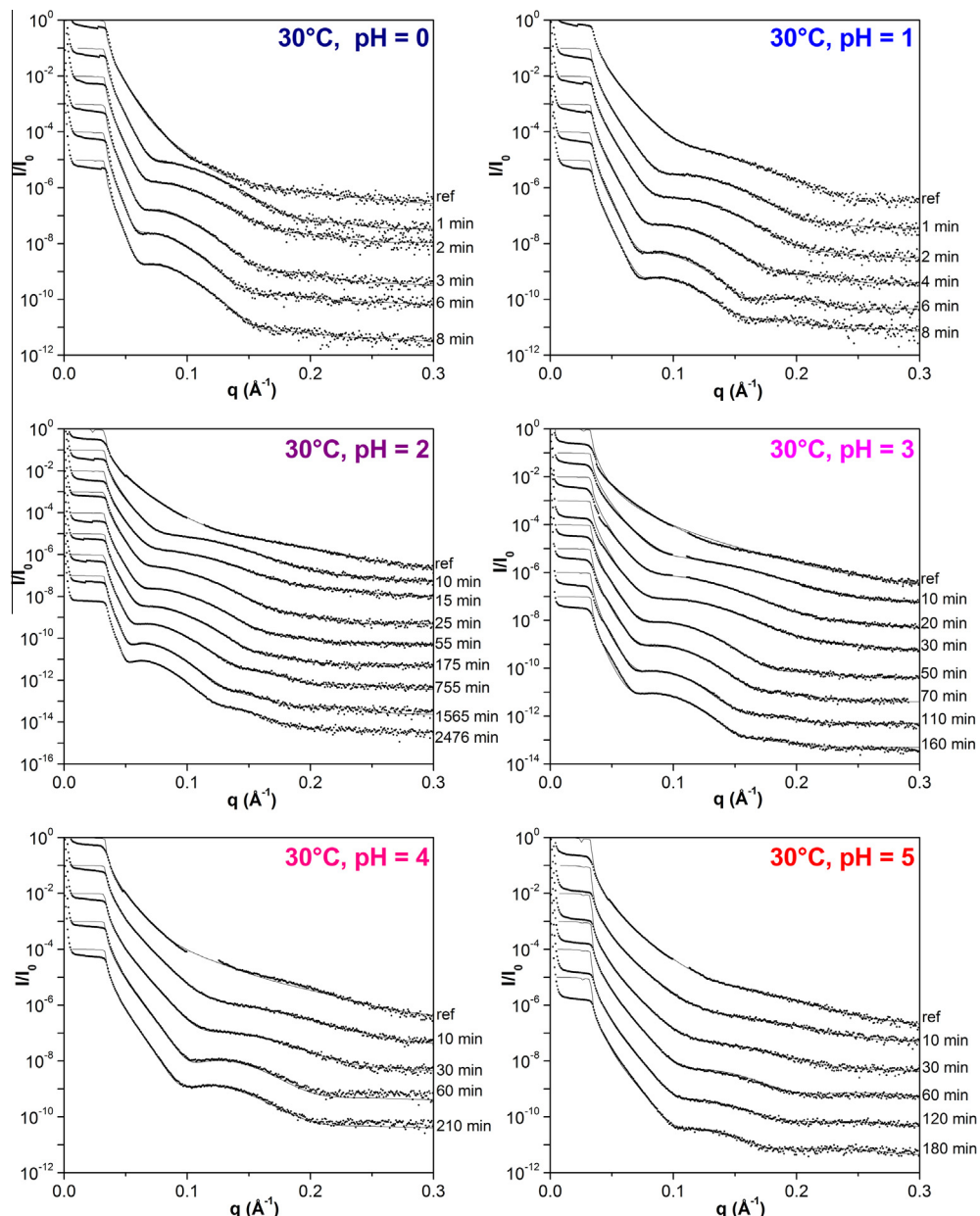
ACKNOWLEDGEMENTS

The authors would like to thank Martiane Cabié from Aix-Marseille University (CP2 M) for help during TEM analyses, Laurent Dupuy from Biophys research for the ToF-SIMS analyses and Bruno Corso from ICSM (LDD) for XRR analyses. Électricité de France (EDF) is gratefully acknowledged for financial support.

APPENDIX A

X-ray Reflectivity curves showing experimental points (dashed lines) and fit data (plain lines) for all experiments.





REFERENCES

- Abrajano T., Bates J., Woodland A., Bradley J. and Bourcier W. (1990) Secondary phase formation during nuclear waste-glass dissolution. *Clay Clay Min.* **38**, 537–548.
- Benzerara K., Menguy N., Banerjee N. R., Tyliszczak T., Brown G. E. and Guyot F. (2007) Alteration of submarine basaltic glass from the Ontong Java Plateau: A STXM and TEM study. *Earth Planet. Sci. Lett.* **260**, 187–200.
- Berger G., Schott J. and Guy C. (1988) Behavior of Li, Rb and Cs during basalt glass and olivine dissolution and chlorite, smectite and zeolite precipitation from seawater: Experimental investigations and modelization between 50 and 300 °C. *Chem. Geol.* **71**, 297–312.

- Berger G., Claparols C., Guy C. and Daux V. (1994) Dissolution rate of a basalt glass in silica-rich solutions – Implications for long-term alteration. *Geochim. Cosmochim. Acta* **58**, 4875–4886.
- Boksay Z., Bouquet G. and Dobos S. (1967) Diffusion processes in surface layers of glass. *Phys. Chem. Glasses* **8**, 140–000.
- Briman I. M., Rebiscoul D., Diat O., Zanotti J.-M., Jollivet P., Barboux P. and Gin S. (2012) Impact of pore size and pore surface composition on the dynamics of confined water in highly ordered porous silica. *J. Phys. Chem. C* **116**, 7021–7028.
- Briman I. M., Rébiscoul D., Diat O., Jollivet P., Zanotti J.-M. and Gin S. (2013) Dynamics of water confined in gel formed during glass alteration at a picosecond scale. *Proc. Earth Planet. Sci.* **7**, 733–737.

- Cailleteau C., Angeli F., Devreux F., Gin S., Jestin J., Jollivet P. and Spalla O. (2008) Insight into silicate-glass corrosion mechanisms. *Nat. Mater.* **7**, 978–983.
- Casey W. and Bunker B. (1990) Leaching of mineral and glass surfaces during dissolution. *Rev. Miner.* **23**, 397–426.
- Chamssedine F., Sauvage T., Peugeot S., Fares T. and Martin G. (2010) Helium diffusion coefficient measurements in R7T7 nuclear glass by $^3\text{He}(\text{d}, \alpha)^1\text{H}$ nuclear reaction analysis. *J. Nucl. Mater.* **400**, 175–181.
- Chave T., Frugier P., Ayral A. and Gin S. (2007) Solid state diffusion during nuclear glass residual alteration in solution. *J. Nucl. Mater.* **362**, 466–473.
- Crovisier J., Honnorez J., Fritz B. and Petit J. (1992) Dissolution of subglacial volcanic glasses from Iceland – Laboratory study and modeling. *Appl. Geochem.*, 55–81.
- Crovisier J. L., Advocat T. and Dussossoy J. L. (2003) Nature and role of natural alteration gels formed on the surface of ancient volcanic glasses (Natural analogs of waste containment glasses). *J. Nucl. Mater.* **321**, 91–109.
- CTDP (2004) Common Thermodynamic Database Project.
- Curti E., Crovisier J. L., Morvan G. and Karpoff A. M. (2006) Long-term corrosion of two nuclear waste reference glasses (MW and SON68): A kinetic and mineral alteration study. *Appl. Geochem.* **21**, 1152–1168.
- Daux V., Guy C., Advocat T., Crovisier J. L. and Stille P. (1997) Kinetic aspects of basaltic glass dissolution at 90 °C: role of aqueous silicon and aluminium. *Chem. Geol.* **142**, 109–126.
- Dohmen L., Lenting C., Fonseca R. O. C., Nagel T., Heuser A., Geisler T. and Denkler R. (2013) Pattern formation in silicate glass corrosion zones. *Int. J. Appl. Glass Sci.* **4**, 357–370.
- Doremus R. H. (1975) Interdiffusion of hydrogen and alkali ions in a glass surface. *J. Non-Cryst. Solids* **19**, 137–144.
- Ebert W. L. and Bates J. K. (1990) The importance of secondary phases in glass corrosion. *MRS Online Proc. Library*, 212.
- Ewing R. C. (1979) Natural glasses: analogues for radioactive waste forms. In *Scientific Basis for Nuclear Waste Management I*. Materials Research Society, pp. 57–66.
- Fares T., Peugeot S., Bouty O., Deschanel X., Magnin M. and Jégou C. (2011) Helium diffusion in curium-doped borosilicate waste glass. *J. Nucl. Mater.* **416**, 236–241.
- Fenter P. and Sturchio N. C. (2004) Mineral-water interfacial structures revealed by synchrotron X-ray scattering. *Prog. Surf. Sci.* **77**, 171–258.
- Fournier M., Gin S. and Frugier P. (2014) Resumption of nuclear glass alteration: State of the art. *J. Nucl. Mater.* **448**, 348–363.
- Frugier P., Gin S., Lartigue J. E. and Deloule E. (2006) SON68 glass dissolution kinetics at high reaction progress: Mechanisms accounting for the residual alteration rate. *MRS Online Proc. Library* **932**.
- Frugier P., Gin S., Minet Y., Chave T., Bonin B., Godon N., Lartigue J.-E., Jollivet P., Ayral A., De Windt L. and Santarini G. (2008) SON68 nuclear glass dissolution kinetics: Current state of knowledge and basis of the new GRAAL model. *J. Nucl. Mater.* **380**, 8–21.
- Galeczka I., Wolff-Boenisch D., Oelkers E. H. and Gislason S. R. (2014) An experimental study of basaltic glass– H_2O – CO_2 interaction at 22 and 50 °C: Implications for subsurface storage of CO_2 . *Geochim. Cosmochim. Acta* **126**, 123–145.
- Geisler T., Janssen A., Scheiter D., Stephan T., Berndt J. and Putnis A. (2010) Aqueous corrosion of borosilicate glass under acidic conditions: A new corrosion mechanism. *J. Non-Cryst. Solids* **356**, 1458–1465.
- Gin S. and Mestre J. P. (2001) SON 68 nuclear glass alteration kinetics between pH 7 and pH 11.5. *J. Nucl. Mater.* **295**, 83–96.
- Gin S., Godon N., Ribet I., Jollivet P., Minet Y., Frugier P., Vernaz E., Cavedon J. M., Bonin B. and Quang R. D. (2004) Long-term behavior of R7T7-type nuclear glass: Current state of knowledge and outlook. In *Scientific Basis for Nuclear Waste Management Xviii* (eds. J. M. Hanchar, S. StroesGascoyne and L. Browning). Materials Research Society, Warrendale, pp. 327–332.
- Gin S., Guittouneau C., Godon N., Neff D., Rebiscoul D., Cabie M. and Mostefaoui S. (2011) Nuclear glass durability: New insight into alteration layer properties. *J. Phys. Chem. C* **115**, 18696–18706.
- Gin S., Beaudoux X., Angélique F., Jégou C. and Godon N. (2012) Effect of composition on the short-term and long-term dissolution rates of ten borosilicate glasses of increasing complexity from 3 to 30 oxides. *J. Non-Cryst. Solids* **358**, 2559–2570.
- Gin S., Abdelouas A., Criscenti L. J., Ebert W. L., Ferrand K., Geisler T., Harrison M. T., Inagaki Y., Mitsui S., Mueller K. T., Marra J. C., Pantano C. G., Pierce E. M., Ryan J. V., Schofield J. M., Steefel C. I. and Vienna J. D. (2013a) An international initiative on long-term behavior of high-level nuclear waste glass. *Mater. Today* **16**, 243–248.
- Gin S., Frugier P., Jollivet P., Bruguier F. and Curti E. (2013b) New insight into the residual rate of borosilicate glasses: Effect of S/V and glass composition. *Int. J. Appl. Glass Sci.* **4**, 371–382.
- Gin S., Ryan J. V., Schreiber D. K., Neeway J. and Cabie M. (2013c) Contribution of atom-probe tomography to a better understanding of glass alteration mechanisms: Application to a nuclear glass specimen altered. *Chem. Geol.* **349**, 99–109.
- Grambow B. (1984) A general rate equation for nuclear waste glass corrosion. *MRS Online Proc. Library*, 44.
- Grambow B. and Muller R. (2001) First-order dissolution rate law and the role of surface layers in glass performance assessment. *J. Nucl. Mater.* **298**, 112–124.
- Guy C. and Schott J. (1989) Multisite surface reaction versus transport control during the hydrolysis of a complex oxide. *Chem. Geol.* **78**, 181–204.
- Gysi A. P. and Stefansson A. (2012) Experiments and geochemical modeling of CO_2 sequestration during hydrothermal basalt alteration. *Chem. Geol.* **306**, 10–28.
- Hellmann R., Wirth R., Daval D., Barnes J.-P., Penisson J.-M., Tisserand D., Epicier T., Florin B. and Hervig R. L. (2012) Unifying natural and laboratory chemical weathering with interfacial dissolution–reciprocation: A study based on the nanometer-scale chemistry of fluid–silicate interfaces. *Chem. Geol.* **294**, 203–216.
- Indris S., Heitjans P., Behrens H., Zorn R. and Frick B. (2005) Fast dynamics of H_2O in hydrous aluminosilicate glasses studied with quasielastic neutron scattering. *Phys. Rev. B* **71**, 64205.
- Jeong G. Y. and Sohn Y. K. (2011) Microtextures, microchemistry, and mineralogy of basaltic glass alteration, Jeju Island, Korea, with implications for elemental behavior. *Am. Miner.* **96**, 1129–1147.
- Jollivet P., Angeli F., Cailleteau C., Devreux F., Frugier P. and Gin S. (2008) Investigation of gel porosity clogging during glass leaching. *J. Non-Cryst. Solids* **354**, 4952–4958.
- Jollivet P., Gin S. and Schumacher S. (2012) Forward dissolution rate of silicate glasses of nuclear interest in clay-equilibrated groundwater. *Chem. Geol.* **330–331**, 207–217.
- Kerisit S. and Liu C. (2009) Molecular simulations of water and ion diffusion in nanosized mineral fractures. *Environ. Sci. Technol.* **43**, 777–782.
- Lasaga A. C. (1981) Transition state theory. *Rev. Mineral. Geochim.* **8**, 135–168.
- Le Gal X., Crovisier J. L., Gauthier-Lafaye F., Honnorez J. and Grambow B. (1999) Meteoric alteration of Icelandic volcanic glass: Long-term changes in the mechanism. *Comptes Rendus Acad. Sci. Ser II-A* **329**, 175–181.

- Libourel G., Verney-Carron A., Morlok A., Gin S., Sterpenich J., Michelin A., Neff D. and Dillmann P. (2011) The use of natural and archeological analogues for understanding the long-term behavior of nuclear glasses. *C. R. Geosci.* **343**, 237–245.
- Lide D. R. ed. (2005) CRC Handbook of Chemistry and Physics, 85th ed. Boca Raton.
- Maeda T., Hotta K., Usui H. and Banba T. (2012) Characteristics of alteration layers formed on simulated HLW glass under silica-saturated solutions. *J. Aust. Ceram. Soc.* **48**, 90–95.
- McGrail B. P., Icenhower J. P., Shuh D. K., Liu P., Darab J. G., Baer D. R., Thevuthasan S., Shutthanandan V., Engelhard M. H., Booth C. H. and Nachimuthu P. (2001) The structure of $\text{Na}_2\text{O}-\text{Al}_2\text{O}_3-\text{SiO}_2$ glass: Impact on sodium ion exchange in H_2O and D_2O . *J. Non-Cryst. Solids* **296**, 10–26.
- Mercado-Depierre S., Angeli F., Frizon F. and Gin S. (2013) Antagonist effects of calcium on borosilicate glass alteration. *J. Nucl. Mater.* **441**, 402–410.
- Minitti M. E., Weitz C. M., Lane M. D. and Bishop J. L. (2007) Morphology, chemistry, and spectral properties of Hawaiian rock coatings and implications for Mars. *J. Geophys. Res. Planets* **112**, E05015.
- Ober R. (raymond.ober@college-de-france.fr) Firefx4c_6.
- Oelkers E. H. and Gislason S. R. (2001) The mechanism, rates and consequences of basaltic glass dissolution: I. An experimental study of the dissolution rates of basaltic glass as a function of aqueous Al, Si and oxalic acid concentration at 25 °C and pH 3 and 11. *Geochim. Cosmochim. Acta* **65**, 3671–3681.
- Parratt L. (1954) Surface studies of solids by total reflection of X-rays. *Phys. Rev.* **95**, 359–369.
- Parruzot B. P. (2014) Altération des verres basaltiques dans des environnements confinés: analogie avec le stockage géologique des verres nucléaires [Basaltic glass alteration in confined environments: analogy to nuclear waste glass geological repository]. Ph.D. thesis, Université Montpellier 2.
- Petit J., Dellamea G., Dran J., Magonthier M., Mando P. and Paccagnella A. (1990a) Hydrated-layer formation during dissolution of complex silicate-glasses and minerals. *Geochim. Cosmochim. Acta* **54**, 1941–1955.
- Petit J., Magonthier M., Dran J. and Dellamea G. (1990b) Long-term dissolution rate of nuclear glasses in confined environments – Does a residual chemical affinity exist. *J. Mater. Sci.* **25**, 3048–3052.
- Poinsot C. and Gin S. (2012) Long-term behavior science. The cornerstone approach for reliably assessing the long-term performance of nuclear waste. *J. Nucl. Mater.* **420**, 182–192.
- Rebiscoul D. (2014) Personal Communication.
- Rebiscoul D., Van der Lee A., Rieutord F., Ne F., Spalla O., El-Mansouri A., Frugier P., Ayral A. and Gin S. (2004) Morphological evolution of alteration layers formed during nuclear glass alteration: New evidence of a gel as a diffusive barrier. *J. Nucl. Mater.* **326**, 9–18.
- Rebiscoul D., Frugier P., Gin S. and Ayral A. (2005) Protective properties and dissolution ability of the gel formed during nuclear glass alteration. *J. Nucl. Mater.* **342**, 26–34.
- Rebiscoul D., Rieutord F., Ne F., Frugier P., Cubitt R. and Gin S. (2007) Water penetration mechanisms in nuclear glasses by X-ray and neutron reflectometry. *J. Non-Cryst. Solids* **353**, 2221–2230.
- Rebiscoul D., Bruguier F., Magnin V. and Gin S. (2012) Impact of soda-lime borosilicate glass composition on water penetration and water structure at the first time of alteration. *J. Non-Cryst. Solids* **358**, 2951–2960.
- Ribet S. and Gin S. (2004) Role of neofomed phases on the mechanisms controlling the resumption of SON68 glass alteration in alkaline media. *J. Nucl. Mater.* **324**, 152–164.
- Scheetz B., Roy D., Tanner C., Barnes M., Gruztek M. and Atkinson S. (1985) Properties of cement-solidified radioactive-waste forms with high levels. *Am. Ceram. Soc. Bull.* **64**, 687–690.
- Schiffman P., Watters R. J., Thompson N. and Walton A. W. (2006) Hyaloclastites and the slope stability of Hawaiian Volcanoes: Insights from the Hawaiian Scientific Drilling Project's 3-km drill core. *J. Volcanol. Geotherm. Res.* **151**, 217–228.
- Stockmann G. J., Wolff-Boenisch D., Gislason S. R. and Oelkers E. H. (2011) Do carbonate precipitates affect dissolution kinetics? I: Basaltic glass. *Chem. Geol.* **284**, 306–316.
- Stronck N. A. and Schmincke H. U. (2001) Evolution of palagonite: Crystallization, chemical changes, and element budget. *Geochem. Geophys. Geosyst.* **2**, 2000GC000102.
- Stronck N. A. and Schmincke H. U. (2002) Palagonite – A review. *Int. J. Earth Sci.* **91**, 680–697.
- Techer I., Advocat T., Lancelot J. and Liotard J. M. (2000) Basaltic glass: Alteration mechanisms and analogy with nuclear waste glasses. *J. Nucl. Mater.* **282**, 40–46.
- Techer I., Advocat T., Lancelot J. and Liotard J. M. (2001) Dissolution kinetics of basaltic glasses: Control by solution chemistry and protective effect of the alteration film. *Chem. Geol.* **176**, 235–263.
- Valle N., Verney-Carron A., Sterpenich J., Libourel G., Deloue E. and Jollivet P. (2010) Elemental and isotopic (Si-29 and O-18) tracing of glass alteration mechanisms. *Geochim. Cosmochim. Acta* **74**, 3412–3431.
- Van der Lee J., De Windt L., Lagneau V. and Goblet P. (2003) Module-oriented modeling of reactive transport with HYTEC. *Comput. Geosci.* **29**, 265–275.
- Van Iseghem P. and Grambow B. (1987) The long-term corrosion and modelling of two simulated Belgian reference high-level waste glasses. *MRS Online Proc. Library*, 112.
- Van Iseghem P. P. V., Timmermans W. and Batist R. D. (1984) Parametric study of the corrosion behaviour in static distilled water of simulated European reference high level waste glasses. *MRS Online Proc. Library*, 44.
- Verney-Carron A., Gin S. and Libourel G. (2010) Archaeological analogs and the future of nuclear waste glass. *J. Nucl. Mater.* **406**, 365–370.
- Verney-Carron A., Vigier N. and Millot R. (2011) Experimental determination of the role of diffusion on Li isotope fractionation during basaltic glass weathering. *Geochim. Cosmochim. Acta* **75**, 3452–3468.
- Walton A. W., Schiffman P. and Macpherson G. L. (2005) Alteration of hyaloclastites in the HSDP 2 Phase 1 Drill Core: 2. Mass balance of the conversion of sideromelane to palagonite and chabazite. *Geochem. Geophys. Geosyst.* **6**, Q09G19.
- Wang J. W., Kalinichev A. G. and Kirkpatrick R. J. (2006) Effects of substrate structure and composition on the structure, dynamics, and energetics of water at mineral surfaces: A molecular dynamics modeling study. *Geochim. Cosmochim. Acta* **70**, 562–582.
- Yanagisawa N., Fujimoto K., Nakashima S., Kurata Y. and Sanada N. (1997) Micro FT-IR study of the hydration-layer during dissolution of silica glass. *Geochim. Cosmochim. Acta* **61**, 1165–1170.
- Yokoyama T. (2013) Characterization of the reaction and transport properties of porous rhyolite and its application to the quantitative understanding of the chemical weathering rate. *Geochim. Cosmochim. Acta* **118**, 295–311.